Design and Simulation of Readout Circuit for Superconductor Nanowire Single Photon Detectors in Cryogenic Environments

by

Buğra Tufan

A Dissertation Submitted to the
Graduate School of Sciences and Engineering
in Partial Fulfillment of the Requirements for
the Degree of

Master of Science

in

Electrical and Electronics Engineering

KOÇ ÜNİVERSİTESİ

August 2, 2024

Design and Simulation of Readout Circuit for Superconductor Nanowire Single Photon Detectors in Cryogenic Environments

Koç University

Graduate School of Sciences and Engineering

This is to certify that I have examined this copy of a master's thesis by

Buğra Tufan

and have found that it is complete and satisfactory in all respects,

and that any and all revisions required by the final

examining committee have been made.

Committee Members:

____

Assoc. Prof. Mehmet Cengiz ONBAŞLI (Advisor)

____

Assoc. Prof. Sedat NİZAMOĞLU

____

Asst. Prof. Kadir DURAK

Date: __________________________________

Dedicated to my precious family.

ABSTRACT

Design and Simulation of Readout Circuit for Superconductor Nanowire Single Photon Detectors in Cryogenic Environments

Master of Science in Electrical and Electronics Engineering

August 2, 2024

This thesis investigates the development of readout circuits for Superconducting Nanowire Single-Photon Detectors (SNSPDs), with a special emphasis on the cryogenic electronics that facilitate their operation near 4.2 Kelvin. SNSPDs exploit the light-driven superconducting-to-resistive phase transition of ultra-thin wires to achieve high detection efficiency, low dark count rates, and ultrafast response times. Photon absorption in these detectors generates a hotspot, disrupting the superconducting state, which is then converted into a measurable electrical signal. A critical design consideration is the proximity of the first-stage preamplifier to the SNSPD to minimize signal loss and optimize load impedance, a strategy that enhances readout effectiveness. However, the challenge lies in designing integrated circuits capable of reliably reading out these signals at such low temperatures.

Traditional silicon-based MOSFETs, commonly used in such circuits, often experience carrier freeze-out at extreme temperatures around 4.2 K, leading to compromised performance. This phenomenon is further exacerbated by issues such as partial doping freeze-out and the freeze-out of parasitic edge transistors, as detailed in recent studies. On the other hand, High Electron Mobility Transistors (HEMTs) have been demonstrated to effectively bypass these limitations, thus proving to be more suitable for use in SNSPD readout circuits. Additionally, the robust performance of GaN HEMT's at temperatures as low as 4.2 K further validates their potential for cryogenic preamplifiers.

In this thesis, the suitability of a cryogenic preamplifier circuit designed using GaN HEMTs for SNSPD sensors has been evaluated through SPICE simulations. The ASM-HEMT model was employed to facilitate the SPICE simulation of the GaN HEMTs. Necessary modifications were made to the ASM-HEMT model to ensure that its behavior aligned with experimental results at cryogenic temperatures.

The simulations revealed that at the typical SNSPD operating frequency of around 1 GHz, a gain of 31.4 dB was achieved, along with a power dissipation of 1.2 mW. This low-power dissipation is crucial for maintaining the thermal budget constraints of dilution refrigerators, making the design scalable for multi-pixel SNSPDs. Additionally, it was observed that GaN HEMTs exhibit significantly lower on-state resistance at cryogenic temperatures compared to room temperature and achieve up to 75% higher $I_{DS,max}$ values, consistent with experimental results. This confirms the superior performance metrics of GaN HEMTs at low temperatures, as reported in the literature. The findings of this thesis suggest that GaN HEMTs are excellent candidates for use in cryogenic preamplifier circuits, providing a foundational approach to enhancing the efficiency and reliability of SNSPD systems.

ÖZETÇE

Kriyojenik Ortamlarda Süperiletken Nanotel Tek-foton Dedektörleri için

Okuma Devresinin

Tasarımı ve Simülasyonu

Elektrik ve Elektronik Mühendisliği, Yüksek Lisans

2 Ağustos 2024

Bu tez, 4.2 Kelvin civarında çalışmayı kolaylaştıran kriyojenik elektroniğe odaklanarak, Süperiletken Nanotel Tek-Foton Dedektörleri (SNSPD'ler) için okuma devrelerinin geliştirilmesini incelemektedir. SNSPD'ler, yüksek tespit verimliliği, düşük karanlık sayım oranları ve ultra hızlı yanıt süreleri sağlamak için ışık kaynaklı süperiletken-iletken faz geçişini kullanır. Foton soğurulması, süperiletken durumu bozarak ölçülebilir bir elektrik sinyaline dönüşen bir sıcak nokta oluşturur. Sinyal kaybını en aza indirmek için preamplifikatörün SNSPD'ye yakın olması önemlidir; ancak, bu sıcaklıklarda güvenilir entegre devreler tasarlamak zordur.

Bu tür devrelerde yaygın olarak kullanılan geleneksel silikon bazlı MOSFET'ler, 4.2 K civarındaki aşırı sıcaklıklarda taşıyıcı donma sorunu yaşayarak performansın düşmesine neden olur. Bu fenomen, kısmi doping donması ve parazitik kenar transistörlerinin donması gibi sorunlarla daha da kötüleşir, bu durum son çalışmalarda detaylandırılmıştır. Öte yandan, Yüksek Elektron Hareketliliği Transistörleri (HEMT'ler), bu sınırlamaları etkili bir şekilde aşarak SNSPD okuma devrelerinde kullanım için daha uygun olduğunu kanıtlamıştır. Ayrıca, GaN HEMT'lerin 4.2 K kadar düşük sıcaklıklarda sağlam performansı, kriyojenik preamplifikatörler için potansiyellerini daha da doğrulamaktadır.

Bu tez kapsamında, GaN HEMT kullanılarak tasarlanan kriyojenik preamplifikatör devresinin SNSPD sensörleri için uygunluğu SPICE simülasyonlarıyla değerlendirilmiştir. GaN HEMT'lerin SPICE simülasyonunu kolaylaştırmak için ASM-HEMT modeli kullanılmış ve ASM-HEMT modelinin kriyojenik sıcaklıklarda deneysel sonuçlarla uyumlu olacak şekilde davranış sergilemesi için gerekli modifikasyonlar yapılmıştır.

Simülasyonlar, tipik SNSPD çalışma frekansı olan 1 GHz civarında 31.4 dB kazanç ve 1.2 mW güç tüketimi elde edildiğini ortaya koymuştur. Bu düşük güç tüketimi, seyreltilmiş soğutucuların termal bütçe kısıtlamalarını korumak için kritik öneme sahiptir ve tasarımın çok pikselli SNSPD'ler için ölçeklenebilir olmasını sağlar. Ayrıca, GaN HEMT'lerin kriyojenik sıcaklıklarda oda sıcaklığına kıyasla önemli ölçüde daha düşük on-state dirence sahip olduğu ve deneysel sonuçlarla tutarlı olarak %75 daha yüksek $I_{DS,max}$ değerlerine ulaştığı gözlemlenmiştir. Bu, literatürde de belirtildiği gibi GaN HEMT'lerin düşük sıcaklıklarda daha yüksek performans metriklerine sahip olduğunu doğrulamaktadır. Bu tez bulguları, GaN HEMT'lerin kriyojenik preamplifikatör devrelerinde kullanım için mükemmel adaylar olduğunu ve SNSPD sistemlerinin verimliliğini ve güvenilirliğini artırmak için temel bir yaklaşım sağladığını önermektedir.

ACKNOWLEDGEMENTS

This thesis is the product of the last two years of study with emotional ups and downs. It is a work that started with lucky coincidences, continued with both disappointments and encouragement from time to time, and was completed thanks to the people who supported.

First, I would like to give my deepest gratitude to my advisor, Assoc. Prof. Mehmet Cengiz Onbaşlı. None of this work would have been possible without his support and guidance. He patiently helped me expand my knowledge in semiconductor physics and contributed significantly to the creation of this work. He provided guidance for obtaining the necessary training and continually accelerated my progress. Without his vision, the applications of this thesis would not have been as fitting.

I would also like to thank Altuğ Somay and Eyüp Erdem Erbil for their technical and moral support during my master's program. Their assistance in difficult times made it much easier for me to solve some of the problems I encountered.

Lastly, this work would not have been possible without the moral support of my dearest family. I am grateful for their eternal support and love. Also, I am thankful to my father for always supporting me in developing myself in the field of engineering since my childhood.

Funding support from the European Research Council (ERC) Starting Grant SKYNOLIMIT with No. 948063 and ERC Proof of Concept Grant SuperPHOTON with No. 101100718 are acknowledged.

TABLE OF CONTENTS

List of Tables ix

List of Figures x

Abbreviations xiii

Chapter 1: Introduction 1

1.1 Background and Motivation 2

1.1.1 Importance of Single Photon Detection 2

1.1.2 Superconductivity 3

1.1.3 Maintaining Superconductivity: The Role of Dilution Refrigerators ... 5

1.1.4 Literature Review: Comparison of Semiconductor Devices for Cryogenic Applications 8

1.2 Contributions of This Thesis 14

1.3 Section of This Thesis 15

Chapter 2: Single-Photon Detection and Cryogenic Readout Electronics 16

2.1 Introduction to Single-Photon Detectors 16

2.1.1 Figures of Merit for Single Photon Detectors 16

2.1.2 Types of Single Photon Detectors 18

2.2 Detailed Study of SNSPDs 24

2.2.1 Working Principle and Physics 24

2.2.2 Design and Function of Readout Circuits 27

Chapter 3: High Electron Mobility Transistor Design for Cryogenic Environments 29

3.1 Key Milestones in the Development of HEMT Devices 29

3.2 Physics of GaN Based HEMT Devices and Related Concepts 31

3.2.1 Heterojunction Formation 31

3.2.2 Two-Dimensional Electron Gas (2DEG) 32

3.2.3 Polarization Effects 34

3.3 Effects of Cryogenic Temperatures on GaN based HEMT Devices 36
3.4 Structural Design of GaN HEMT for Cryogenic Preamplifier 38
3.5 SPICE Simulation of GaN HEMT Device 40
3.5.1 DC Analysis of HEMT at Room Temperature 42
3.5.2 Applying Required Modifications to ASM-HEMT for Cryogenic Temperatures 46
3.6 Layout Design of GaN HEMT Device 51
3.7 Conclusion 53
Chapter 4: Design and Integration of SNSPD Readout Circuit 54
4.1 Overview of SNSPD Sensor Modeling 56
4.2 Preamplifier Design Integration 58
Chapter 5: Conclusion and Future Work 62
5.1 Summary of Findings 62
5.2 Recommendations for Future Research 64
Bibliography 67
Appendix A: KLayout Scripts for 2D GDS File Generation and 2.5D Visualization 80

LIST OF TABLES

Table 1.1: Dilution refrigerator specifications. Temperatures and available cooling powers on the indicated stages of a Bluefors XLD400 DR. [25] 7

Table 1.2: Comparison of Semiconductor Device Features in Cryogenic Temperatures 13

Table 2.1: Comprehensive Overview of Single-Photon Detector Specifications from Literature, PNR: Photon Number Resolvability 24

Table 3.1: Comparison of Material Properties of Si and GaN 37

Table 3.2: The extracted parameters for the device. [94] 47

Table 4.1: Comparison of Cryogenic Preamplifier Gain and Power Consumption Across Various Studies 61

Table 5.1: Some of the GaN foundries that provide growth and fabrication services for GaN-based epilayers and devices 64

LIST OF FIGURES

Figure 1.1: Resistance versus temperature curve of superconductors and normal conductors. [18] 4

Figure 1.2: Critical surface of a superconductor. [24] 5

Figure 1.3: Cabled dilution refrigerator (DR). (a) Bluefors XLD DR with 25 drive lines, 25 flux lines, 4 read-out, 6 read-in, and 5 pump lines installed. (b) Schematic of the cabling configuration within the DR. [25] 6

Figure 1.4: Schematic cross section of SiGe HBT on wafer-bonded SOI with buried silicide collector layer and buried silicide groundplane. © 2005 IEEE. Reprinted, with permission, from M. Bain et al., "SiGe HBTs on bonded SOI incorporating buried silicide layers," in IEEE Transactions on Electron Devices, vol. 52, no. 3, pp. 317-324 9

Figure 1.5: An operating GaAs MESFET showing three different regions of the gate depletion. Region-I & III are due to the extension of gate depletion in the gate-source and gate-drain sides respectively. © 2013 IEEE. Reprinted, with permission, from M. M. Ahmed, N. M. Memon and S. A. Moiz, "Effects of interfacial layer on submicron GaAs MESFETs characteristics," 2013 IEEE 9th International Conference on Emerging Technologies (ICET), Islamabad, Pakistan 10

Figure 1.6: AlGaN/InGaN/GaN HEMT structure. [41]... 12

Figure 2.1: Detection efficiency as a function of time 17

Figure 2.2: Ge-on-Si single-photon avalanche diode (SPAD) structure. [47]......... 19

Figure 2.3: Transition Edge Sensor Schematic. [53] 21

Figure 2.4: (a) Schematic of quasi-constant-current-bias circuit for SNSPD. (b) Current-voltage curve of SNSPD without light. Solid arrows indicate the up sweep curve from 0 to 1.5 V. Dash arrows indicate the down sweep from 1.5 to 0 V. [67] 25

Figure 2.5: Schematics of the supercurrent-assisted hotspot formation mechanism in an ultrathin and narrow superconducting strip, kept at temperature far below TC are shown. The arrows indicate direction of the supercurrent flow. [58] 26

Figure 3.1: Timeline of Key Milestones in the Development of High Electron Mobility Transistors (HEMTs) 30

Figure 3.2: Structure of AlGaN/GaN HEMT © 2019 IEEE. Reprinted, with permission, from J. C. Choton, A. Begum and J. K. Saha, "Design and Characterization of 2DEG Structure of a Gallium Nitride HEMT," 2019 International Conference on

Robotics,Electrical and Signal Processing Techniques (ICREST), Dhaka, Bangladesh, 2019, pp. 486-489 32

Figure 3.3: Simplified AlGaAs/GaAs HEMT structure, (b) corresponding band diagram. [104] 33

Figure 3.4: Electric field and sheet charges present (a) due to only spontaneous polarization in GaN and AlGaN crystals; and (b) due to only piezoelectric polarization in a AlGaN layer. 35

Figure 3.5: (a) Schematic diagram of GaN-based HEMT. (b) The test platform for temperature-dependent DC and LFN characterizations, including the probe station, semiconductor analyzers, and liquid helium dewar. [94] 38

Figure 3.6: DC characteristics of the DUT under various T: output characteristics at (a) 300 K and (b) 4.2 K. (c) Comparison of the output curves at VGS = 1 V from 300 K to 4.2 K. Extracted (d) IDS, max and (e) RON as a function of T from the output curves. [94] 39

Figure 3.7: Steps Involved in Simulating GaN HEMT with Ngspice 41

Figure 3.8: Circuit Diagram for DC analysis of HEMT 43

Figure 3.9: DC characteristics of the DUT at room temperature with a device length of 50 µm: output characteristics for gate widths of (a) 1 µm, (b) 3 µm, and (c) 7 µm with VGS varying from 0V to -5V. 44

Figure 3.10: DC characteristics of the DUT at room temperature with a gate width of 3 µm: output characteristics for device lengths of (a) 50 µm, (b) 75 µm, and (c) 100 µm with VGS varying from 0V to -5V. 45

Figure 3.11: Characterizing Low Field Mobility Across Temperature Ranges 46

Figure 3.12: DC characteristics of the DUT at 4.2 Kelvin with a gate width of 3 µm and a device length of 50 µm. (a) shows the output characteristics using the unmodified ASM-HEMT model, while (b) displays the improved results with the modified ASM-HEMT model, indicating a 75% increase in IDS, max value from 28 mA to 49 mA. .. 48

Figure 3.13: DC characteristics of the DUT at 4.2 Kelvin with a device length of 50 µm: output characteristics for gate widths of (a) 3 µm, and (b) 7 µm with VGS varying from 0V to -5V. 49

Figure 3.14: Voltage Response of $Vdrain, rd$ Across RD to Changes in $Vgate$... 50

Figure 3.15: Frequency-Dependent Behavior of Drain Voltage in Modified ASM-HEMT on a Logarithmic Scale at 4.2 Kelvin 51

Figure 3.16: 2D Top View of Designed GaN HEMT Device 52

Figure 3.17: 2.5D View of Designed HEMT Device 52

Figure 4.1: A simple electrical equivalent circuit of a SNSPD. Lk is the kinetic inductance of the superconducting nanowire and Rn is the hotspot resistance of the SNSPD. The SNSPD is current biased at $Ibias$. Opening and closing the switch simulates the absorption of a photon. An output pulse is measured across the load resistor $Z0$. [99] 56

Figure 4.2: Time-Domain Simulation of Photon Detection in the SNSPD Equivalent Circuit Using SPICE. $V(Z0)$represents the voltage difference across $Z0$...................... 56

Figure 4.3: Time-Domain Simulation of Photon Detection in the SNSPD Equivalent Circuit with Different Rise Time 57

Figure 4.4: Frequency domain analysis of SNSPD signals with different rise times. Region I shows the meaningful part of the signal, while Region II captures the high-frequency noise caused by the steep rise of the signals. 58

Figure 4.5: (a) Circuit schematics implementing HEMT amplifier and 500 Ohm load resistor. The 10-nF capacitor sets the maximum ac gain and a 200 Ohm resistor sets the dc current for the HEMT; and are the biasing and pull-up resistors, respectively. (b) Standard electrical photoresponse model of the SSPD with S denoting the detector switching action. Z_0=50 Ohm [103] 59

Figure 4.6: Frequency Response of Cryogenic GaN HEMT Amplifier 60

ABBREVIATIONS

SNSPD	Superconductor Nanowire Single Photon Detector
SPD	Single Photon Detector
TES	Transition Edge Sensor
HEMT	High Electron Mobility Transistor
MOSFET	Metal-Oxide-Semiconductor Field-Effect Transistor
MESFET	Metal-Semiconductor Field-Effect Transistor
HBT	Heterojunction Bipolar Transistor
CMOS	Complementary Metal-Oxide-Semiconductor
Si	Silicon
SiGe	Silicon-Germanium
GaAs	Gallium Arsenide
GaN	Gallium Nitrate
2DEG	Two-Dimensional Electron Gas
PNR	Photon Number Resolvability
STJ	Superconducting Tunnel Junction
DR	Dilution Refrigerator
SNR	Signal-to-Noise Ratio
LFN	Low Frequency Noise
LNA	Low Noise Amplifier
SPICE	Simulation Program with Integrated Circuit Emphasis
AC	Alternative Current
DC	Direct Current
RF	Radio Frequency
K	Kelvin
mK	Millikelvin
OSDI	Open Simulation Device Interface
PDK	Process Design Kit
DIBL	Drain-Induced Barrier Lowering

Chapter 1:
INTRODUCTION

Quantum computing has emerged as a revolutionary paradigm in computing, offering unprecedented capabilities for solving complex problems beyond the reach of classical computers. In recent years, significant advances have been made in quantum computing research, bringing practical quantum computers closer to reality [1]. These advances have led to increasing applications in sensing and computation technologies.

As quantum computing applications continue to gain traction, the demand for efficient and reliable readout circuits has become increasingly important. A key challenge in developing practical quantum computing systems is their operation at cryogenic temperatures, typically below 4K [2]. This requirement arises from the need to operate quantum computing applications in extremely stable mechanical and thermal environments because thermal energy can excite vibrational motion that could disturb quantum computing operations [3]. Consequently, there is a growing need for electronic devices and integrated circuits capable of functioning effectively in such extreme conditions. Conventional electronic materials and devices, such as silicon-based metal-oxide-semiconductor field-effect transistors (MOSFETs), often exhibit performance degradation and increased power consumption at cryogenic temperatures [4]. This has driven researchers to explore alternative materials and device structures that can provide reliable operation and improved performance in these environments. Among the various candidates, GaN High Electron Mobility Transistor (HEMT) has emerged as a promising material for cryogenic electronics due to its unique properties [5][6][7].

In this chapter, I introduce the background and motivation for the research. I explain the fundamental concepts, including the importance of single-photon detection. I also discuss superconductivity, the role of dilution refrigerators in maintaining superconductivity, and a literature review that compares semiconductor devices for cryogenic applications. Finally, I highlight the contributions of this thesis and provide an overview of the subsequent chapters.

1.1 Background and Motivation

1.1.1 Importance of Single Photon Detection

The fundamental quantum of light, a photon, is the smallest physical entity in the electromagnetic spectrum. Its detection is crucial for experimental physics, where the ability to accurately measure single photons enables advancements across various scientific fields, such as quantum computation, quantum communication, and deep-space observations [8][9][10][11]. Photodetectors are the instruments that make photon detection possible, serving a crucial role in our ability to engage with the quantum domain. These detectors, ranging from semiconductors to superconductors, are adept at capturing incoming light signals and converting them into electrical signals that we can measure and analyze. This conversion is vital for various applications that rely on precise and discernible detection of photons.

Photon detection technology has been subject to a significant evolution, commencing with the early adoption of photomultiplier tubes (PMTs) [12], which revolutionized time-correlated photon-counting techniques (TCPC). This technology provided unparalleled sensitivity within its spectral range, enabling precise measurements of weak and transient fluorescence signals. By the late 1970s, a technological leap occurred with the development of avalanche photodiodes, or more specifically, single-photon avalanche diodes (SPADs) [13]. These devices, biased above their breakdown voltage, signified a more affordable and compact alternative to PMTs, capable of operating up to near-infrared wavelengths and applicable in a multitude of disciplines, including spectroscopy and quantum-mechanical interference studies at the single-photon level.

With the continuous quest for enhanced quantum efficiency and the need to resolve photon numbers with precision, superconducting devices entered the scene. Transition edge sensors (TES) are one such innovation, leveraging the precise temperature dependence of superconducting materials to detect single photons with remarkable accuracy [14]. A TES functions as a highly sensitive microcalorimeter, gauging the quantity of heat absorption. Such a device typically includes an energy absorber, a thermometer to register the resultant temperature rise from energy absorption, and a thermal connection that facilitates the return of the absorber to its foundational temperature after the temperature measurement of the device is finalized [15].

Among the technologies utilizing superconductive properties, Superconducting Nanowire Single-Photon Detectors (SNSPDs) also find their place as a notable sensor. This device capitalizes on the superconducting state of ultra-thin wires, usually only a few nanometers thick. When a photon hits the nanowire, it produces a localized hotspot, disrupting the superconducting state and resulting in a measurable electrical signal. SNSPDs are known for their high detection efficiency, low dark count rates, and fast response times, making them highly effective for applications requiring rapid and accurate single-photon detection [16].

1.1.2 Superconductivity

Superconductivity is a quantum mechanical phenomenon characterized by the absence of electrical resistance and the expulsion of magnetic fields when a material is cooled below a critical temperature (T_c). In this state, electrical current can flow without energy loss, making it highly significant for various technological applications.

The phenomenon of superconductivity was first observed in 1911 by Dutch physicist Heike Kamerlingh Onnes [17]. He discovered that the electrical resistance of mercury dropped to zero when the temperature was reduced to 4.15 Kelvin (-269°C). This discovery marked the identification of superconductivity in certain materials under low-temperature conditions.

All materials can conduct electricity to some extent, but their effectiveness varies widely. Metals, known for their low resistance, allow electric currents to flow easily, while insulators offer high resistance. In normal conductors, electric current is visualized as electrons moving through a lattice of heavy ions. Electrons frequently collide with these ions, converting some of the current's energy into heat, a process known as electrical resistance, leading to energy dissipation.

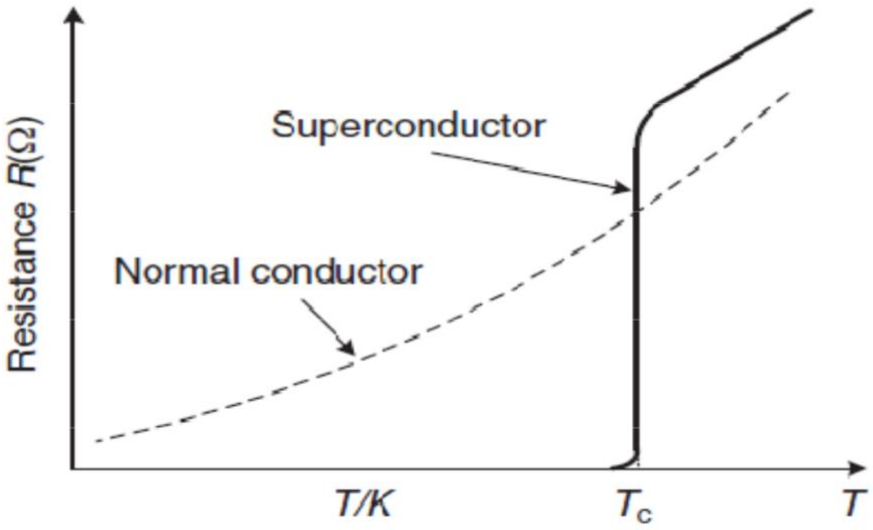

Figure 1.1: Resistance versus temperature curve of superconductors and normal conductors. [18]

However, superconductors exhibit a fundamentally different behavior. As shown in Figure 1, the resistance of superconductors drops to zero below a critical temperature, unlike normal conductors which maintain a finite resistance. [19][20]

In superconductors, electrons form pairs known as Cooper pairs due to an attractive force mediated by phonons, the quantized vibrations of the lattice. Quantum mechanically, the Cooper pair fluid has an energy gap, meaning a minimum energy is required to excite it. If the thermal energy (given by kBT, where B is Boltzmann's constant and T is temperature) is less than this energy gap, the Cooper pairs will not scatter off the lattice, thus allowing the fluid to flow without resistance. This phenomenon, responsible for zero electrical resistance in superconductors, is described in the BCS theory by John Bardeen, Leon Cooper, and Robert Schrieffer, for which they were awarded the Nobel Prize in 1972 [21].

The concept of Cooper pairs was first introduced by Leon Cooper in 1956 [22]. According to Cooper, the attraction between electrons in a metal can lead to a lower energy state for the pair compared to individual electrons at the Fermi level, thus binding the pair. This binding force in conventional superconductors is due to electron-phonon interactions. The BCS theory elaborates on how these pairs lead to superconductivity.

Soon after discovering superconductivity, Kamerlingh Onnes realized its potential for creating high magnetic fields without energy dissipation. However, in 1913, he discovered that superconductivity is destroyed when exposed to small magnetic fields.

Each superconductor has a characteristic critical magnetic field (B_c) which is maximal at 0 Kelvin and decreases with increasing temperature, becoming zero at T_c. In 1916, Francis Silsbee proposed that superconductors also have a critical current (I_c) which, when exceeded, generates a self-field equivalent to B_c, thus destroying superconductivity [23].

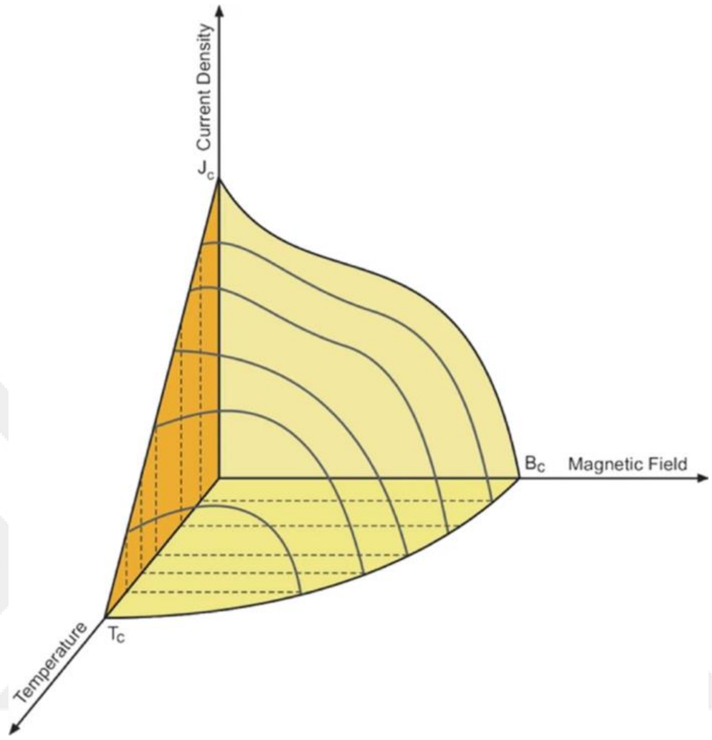

Figure 1.2: Critical surface of a superconductor. [24]

Therefore, three critical parameters characterize a superconductor: critical temperature (T_c), critical field (B_c), and critical current (I_c). These parameters are interdependent and define the superconducting state within their bounds, as illustrated in Figure 1.2.

1.1.3 Maintaining Superconductivity: The Role of Dilution Refrigerators

Superconducting devices rely on ultra-low temperatures to exhibit their remarkable properties, such as zero electrical resistance and the expulsion of magnetic fields. Achieving these temperatures requires advanced cooling systems, with dilution refrigerators being a critical component. These refrigerators use the unique properties of helium-3 and helium-4 mixtures to reach temperatures below 10 millikelvin (mK), essential for various applications in quantum computing and fundamental physics research.

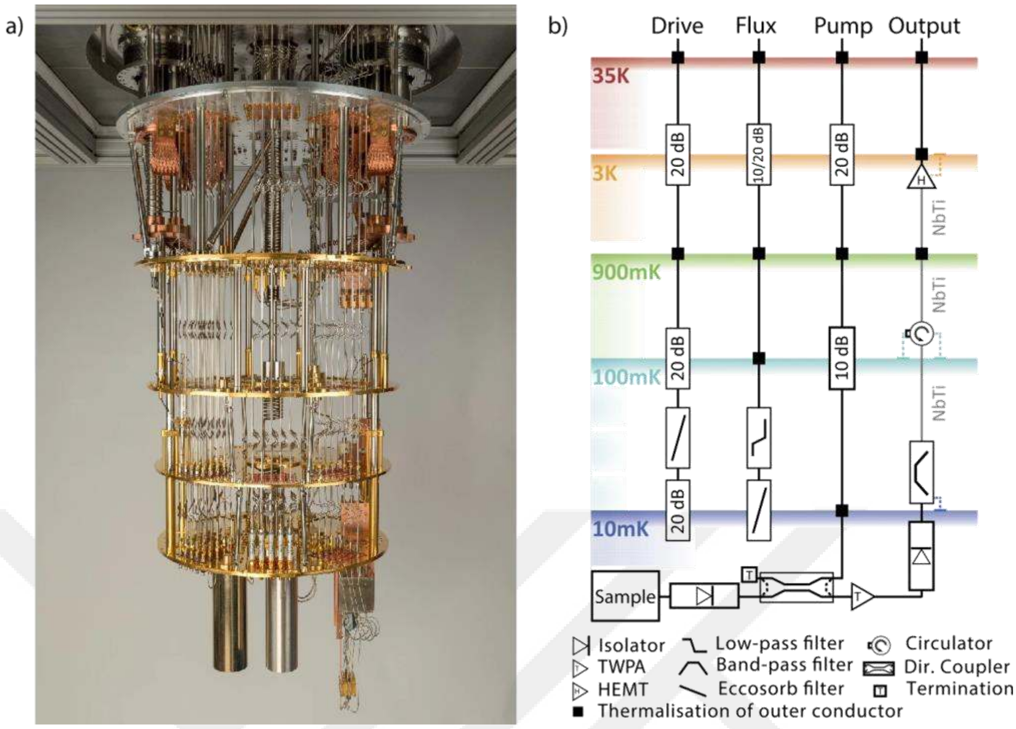

Figure 1.3: Cabled dilution refrigerator (DR). (a) Bluefors XLD DR with 25 drive lines, 25 flux lines, 4 read-out, 6 read-in, and 5 pump lines installed. (b) Schematic of the cabling configuration within the DR. [25]

Dilution refrigerators, such as the Bluefors BF-XLD-SERIES [26], operate without the need for liquid cryogens, making them cryogen-free systems. They utilize the heat of mixing between helium-3 and helium-4 isotopes to achieve ultra-low temperatures. The cooling process begins with the separation of the helium mixture into two phases below 0.8 K: a helium-3 rich concentrated phase and a helium-3 poor dilute phase. The energy required to transfer helium-3 atoms from the concentrated phase to the dilute phase is absorbed from the surrounding environment, resulting in effective cooling of the mixing chamber. Bluefors' cryogen-free design incorporates a pulse tube cooler to initiate the dilution cycle, providing continuous and efficient cooling without the need for traditional liquid helium baths.

The Bluefors BF-XLD-SERIES dilution refrigerator, for example, demonstrates this advanced technology. It achieves temperatures below 10mK through the efficient mixing and separation of helium isotopes. This system, detailed in Figure 1.3, highlights the complexity and precision of modern dilution refrigerators. The schematic shows multiple layers and cabling configurations, including 25 drive lines, 25 flux lines, 4 read-out lines, 6 read-in lines, and 5 pump lines, which are essential for the operation of quantum devices.

Table 1.1: Dilution refrigerator specifications. Temperatures and available cooling powers on the indicated stages of a Bluefors XLD400 DR. [25]

Stage name	Temperature (K)	Cooling power (W)
50 K	35	30 (at 45 K)
4 K	2.85	1.5 (at 4.2 K)
Still	882×10^{-3}	40×10^{-3} (at 1.2 K)
CP	82×10^{-3}	200×10^{-6} (at 140 mK)
MXC	6×10^{-3}	19×10^{-6} (at 20 mK)

One of the challenges in using dilution refrigerators is the potential signal loss at various stages due to connectors and transitions between different temperature layers. These losses can impact the performance of superconducting devices, necessitating careful design and engineering to minimize signal degradation [27].

Additionally, devices and sensors within the dilution refrigerator must remain below certain power dissipation limits, which are related to the cooling power of the refrigerator. For example, Table 1.1 shows the cooling power available at different temperature stages of the Bluefors XLD400 DR. Ensuring that power dissipation stays within these limits is critical to achieving the desired temperatures at each stage of the dilution fridge.

In conclusion, dilution refrigerators are indispensable for maintaining the superconducting properties of devices at ultra-low temperatures. By leveraging the unique properties of helium-3 and helium-4 mixtures, these systems provide stable and efficient cooling, essential for advancing technologies in quantum computing and low-temperature physics. As the demand for high-performance superconducting devices continues to grow, the role of dilution refrigerators in ensuring optimal operating conditions will remain crucial, driving further innovation and development in cryogenic engineering.

1.1.4 Literature Review: Comparison of Semiconductor Devices for Cryogenic Applications

Superconducting Nanowire Single Photon Detectors (SNSPDs) require efficient readout circuits to convert the weak electrical signals generated by photon detection events into readable data while maintaining signal integrity. Traditional readout amplifiers tend to be large and consume significant power, making them difficult to integrate with SNSPDs. As noted in the literature, these amplifiers typically operate at room temperature and are connected to the SNSPDs in cryogenic environments via long coaxial cables. This setup not only limits the size and scalability of SNSPD readout systems but also deteriorates signal quality and introduces significant signal jitters. To address these issues, placing the readout amplifier in the cryogenic environment itself is preferred, resulting in a compact SNSPD readout system that reduces insertion loss and signal interference while maintaining low power consumption [28].

This section explores the performance of various semiconductor devices at cryogenic temperatures, including Si-based MOSFETs, SiGe HBTs, GaAs MESFETs, and GaN HEMTs, to identify the most suitable technology for designing readout preamplifiers for SNSPDs.

Si Based MOSFETs

Traditional silicon-based MOSFETs are commonly used in electronic circuits due to their well-established manufacturing processes and wide availability. However, these devices often experience carrier freeze-out at extreme temperatures around 4 Kelvin, leading to compromised performance. This phenomenon is further exacerbated by issues such as partial doping freeze-out and the freeze-out of parasitic edge transistors, as detailed in recent studies [29].

Moreover, at temperatures below 150 K, the corner effect becomes significant, characterized by a lower threshold voltage at the device corners compared to the top and sidewall Si/SiO_2 interfaces [30]. This leads to a narrower linear region, with the subthreshold slope varying linearly with temperature, ultimately resulting in a reduced subthreshold slope and decreased gain performance at cryogenic temperatures.

Due to these limitations Si-based MOSFETs are not preferred for use at cryogenic temperatures. Instead, alternative semiconductor technologies are being explored to achieve better performance in such extreme conditions.

SiGe HBT

A Silicon-Germanium Heterojunction Bipolar Transistor (SiGe HBT) is a type of bipolar junction transistor (BJT) that utilizes a silicon-germanium alloy in the base region to improve performance. Unlike conventional silicon BJTs, SiGe HBTs benefit from the unique properties of the SiGe material, which allows for better control over the bandgap and enhances carrier mobility. This heterojunction between the silicon emitter and the SiGe base creates a high-performance device capable of operating at higher speeds and frequencies with lower noise. SiGe HBTs are particularly advantageous in high-frequency applications such as RF and microwave communications, as well as in high-speed digital circuits. The incorporation of germanium into the silicon lattice enables these transistors to offer superior performance in terms of gain, bandwidth, and thermal stability compared to traditional silicon BJTs.

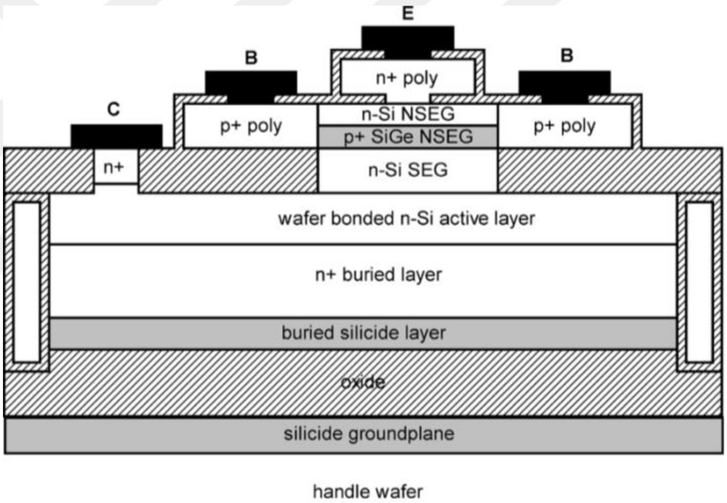

Figure 1.4: Schematic cross section of SiGe HBT on wafer-bonded SOI with buried silicide collector layer and buried silicide groundplane. © 2005 IEEE. Reprinted, with permission, from M. Bain et al., "SiGe HBTs on bonded SOI incorporating buried silicide layers," in IEEE Transactions on Electron Devices, vol. 52, no. 3, pp. 317-324

In Figure 1.4, the schematic cross-section of a SiGe HBT on a wafer-bonded Silicon-On-Insulator (SOI) substrate with a buried silicide collector layer and buried silicide groundplane is shown. This structure highlights the advanced design and fabrication techniques used to enhance the performance and integration of SiGe HBTs in modern semiconductor technologies. The figure illustrates the key layers, including the n-Si active layer, n+ buried layer, buried silicide layer, and the handle wafer, which together contribute to the device's high efficiency and functionality.

Among the various candidates, silicon-germanium (SiGe) has emerged as a promising material for cryogenic electronics due to its unique properties and compatibility with established semiconductor fabrication processes [31][32][33][34].

Despite their advantages, SiGe HBTs also exhibit certain non-ideal behaviors, including high-injection heterojunction barrier effects. These effects tend to worsen with cooling, potentially limiting the use of SiGe HBTs in cryogenic applications [35][36]. Additionally, there is significant uncertainty regarding SiGe HBT characteristics at very low temperatures, making their performance somewhat unpredictable under these conditions [37].

Another drawback of SiGe HBTs is the phenomenon of transconductance saturation that occurs at temperatures below 40 K. This saturation implies that the slope of the collector current no longer increases, and carriers begin to move through a quasi-ballistic transport mechanism, leading to higher power consumption at cryogenic temperatures [38].

Overall, while SiGe HBTs offer several benefits for cryogenic applications, such as high-speed operation and compatibility with existing fabrication processes, their non-ideal behaviors and uncertainties at cryogenic temperatures necessitate careful consideration for their use in specific applications.

GaAs MESFET

Metal-Semiconductor Field-Effect Transistor (MESFET) is a type of FET where the current flow between the source and drain terminals is controlled by a voltage applied to the gate terminal.

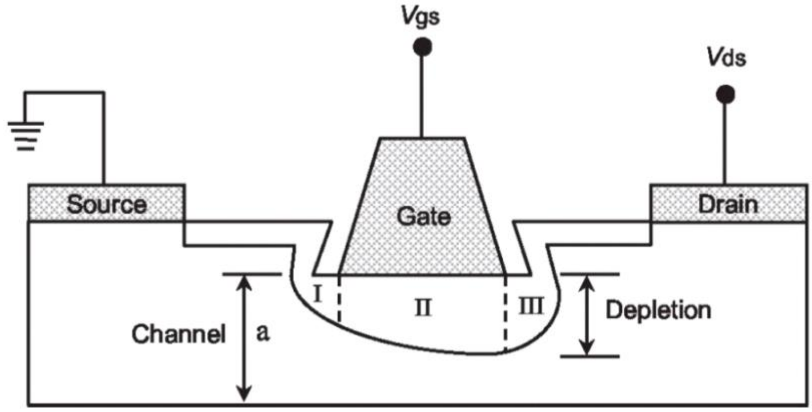

Figure 1.5: An operating GaAs MESFET showing three different regions of the gate depletion. Region-I & III are due to the extension of gate depletion in the gate-source and

gate-drain sides respectively. © 2013 IEEE. Reprinted, with permission, from M. M. Ahmed, N. M. Memon and S. A. Moiz, "Effects of interfacial layer on submicron GaAs MESFETs characteristics," 2013 IEEE 9th International Conference on Emerging Technologies (ICET), Islamabad, Pakistan

Unlike traditional FETs that use an oxide layer between the gate and the channel, MESFETs have a Schottky metal gate directly on the semiconductor channel. This metal-semiconductor junction creates a depletion region that controls the flow of electrons. In Figure 1.5, the schematic of a GaAs MESFET structure is shown, illustrating the depletion region and the Schottky metal gate.

MESFETs are typically fabricated on compound semiconductor materials like Gallium Arsenide (GaAs). Gallium Arsenide (GaAs) MESFETs are known for their high electron mobility and robust performance, making them suitable for high-frequency and low-noise applications. These characteristics are especially beneficial in cryogenic environments, where traditional silicon-based devices often struggle. GaAs MESFETs exhibit stable operation at extremely low temperatures, including those as low as 1.6 K, which further validates their potential for use in cryogenic preamplifiers [39]. Their ability to maintain performance under such conditions makes them a strong candidate for integration into SNSPD readout circuits. Additionally, the inherent low-noise properties of GaAs MESFETs contribute to enhancing the signal integrity and reducing the overall noise floor, which is critical in applications requiring high precision and sensitivity.

GaN HEMT

The recent interest in GaN (Gallium Nitride) has been driven by its exceptional material characteristics, including a high critical electric field, high saturation velocity, high electron mobility, and outstanding thermal stability. These properties make GaN-based high electron mobility transistors (HEMTs) particularly attractive for advanced electronic applications [40].

Gallium Nitride High Electron Mobility Transistors (GaN HEMTs) are advanced semiconductor devices that offer superior performance in high-frequency and high-power applications. The key advantage of GaN HEMTs lies in their heterostructure, typically composed of AlGaN/GaN layers, which facilitates the formation of a two-dimensional electron gas (2DEG) at the interface. This 2DEG results in high electron mobility and high saturation velocity, allowing for efficient and fast electronic switching.

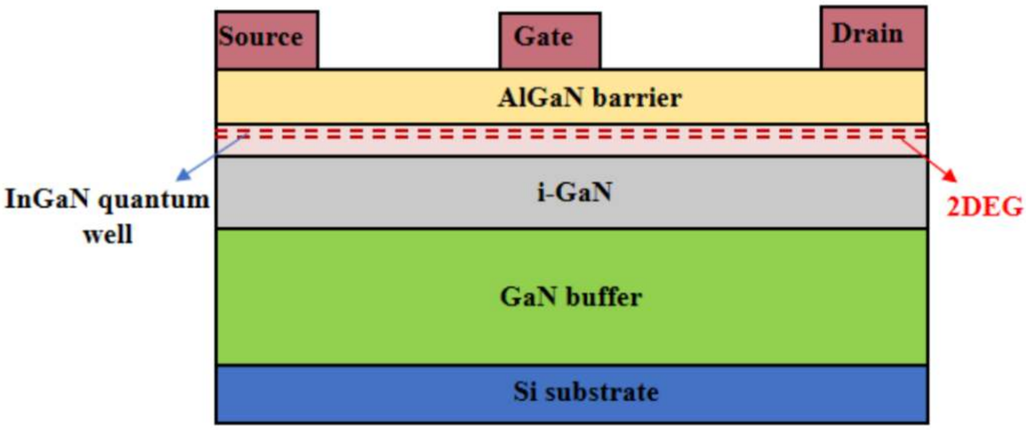

Figure 1.6: AlGaN/InGaN/GaN HEMT structure. [41]

In Figure 1.6, an example of HEMT structure is shown, illustrating the key layers 2DEG that contribute to its high performance.

GaN HEMTs are especially well-suited for cryogenic environments due to their superior performance, which includes maintaining high mobility and low noise at very low temperatures. For low-noise amplifier applications, HEMTs are generally recognized as the best choice, outperforming MESFETs at the same gate length and higher frequencies [42]. This makes HEMTs ideal for high-frequency applications where minimal signal degradation and noise are crucial.

GaN HEMTs also feature a wider bandgap compared to GaAs, which enhances their reliability in environments with energetic radiation and provides a considerably lower noise figure [43]. This wide bandgap results in improved sensitivity and time resolution, critical factors for high-precision applications such as those involving SNSPDs.

Moreover, GaN HEMTs offer lower power dissipation due to their higher mobility and lower resistance, which are results of their high electron carrier concentration and high conductivity [44]. Despite GaN's lower thermal conductivity compared to silicon, its high charge carrier concentration compensates by providing low resistance and efficient operation even at low temperatures. This makes GaN HEMTs a highly promising candidate for preamplifiers in cryogenic readout circuits for SNSPDs.

Table 1.2: Comparison of Semiconductor Device Features in Cryogenic Temperatures

Semiconductor Device	Material	Key Advantages	Behavior at Cryogenic Temperatures	Typical Applications
Si-MOSFET	Silicon	Well-established manufacturing, wide availability	Carrier freeze-out at very low temperatures (4K), doping issues, performance degradation	General electronic circuits not requiring extreme temperature performance
SiGe MOSFET	Silicon-Germanium	Improved bandgap control, higher carrier mobility, enhanced gain and bandwidth	Non-ideal behaviors such as high-injection heterojunction barrier effects, transconductance saturation below 40K	High-frequency applications like RF and microwave communications, high-speed digital circuits
GaAs MESFET	Gallium Arsenide	High electron mobility, robust performance, low-noise characteristics	Stable performance at extremely low temperatures (as low as 1.6K)	High-frequency, low-noise applications, cryogenic preamplifiers including SNSPD readout circuits
GaN HEMT	Gallium Nitride	High mobility and low noise at very low temperatures, improved sensitivity due to wide bandgap, high electron carrier concentration, and high conductivity	Exhibits stable electrical performance and lower noise characteristics at low temperatures. Efficient operation due to low power dissipation and robustness against thermal fluctuations	High-frequency and high-power applications, low-noise amplifier applications including SNSPD readout circuits

1.2 *Contributions of This Thesis*

In this thesis, I designed a GaN HEMT, modified the ASM-HEMT model for operation at cryogenic temperatures, and performed SPICE simulations using ngspice. Subsequently, I designed a preamplifier circuit utilizing the designed HEMT with an SNSPD model and conducted SPICE simulations to analyze its performance. All these tasks were accomplished using open-source tools and workflows.

- **ASM-HEMT Model Modifications:** I extended the existing ASM-HEMT model to operate effectively at cryogenic temperatures. This involved developing a new physics-based compact model incorporating temperature-dependent parameters such as mobility, threshold voltage, and flicker noise.

- **SPICE Simulations:** Using ngspice, I conducted SPICE simulations of the developed model. These simulations were validated against experimental data to ensure accuracy, showing improved performance (increased mobility, reduced on-resistance, and enhanced noise performance) at cryogenic temperatures.

- **Preamplifier Design with SNSPD:** Utilizing the designed GaN HEMT, I integrated it with a Superconducting Nanowire Single-Photon Detector (SNSPD) model to design a preamplifier circuit. I performed SPICE simulations of this circuit and analyzed the results, demonstrating successful operation at cryogenic temperatures and compatibility with SNSPD.

- **Open-Source Tools and Workflows:** All the modeling, design, and simulation tasks were carried out using open-source tools and workflows, ensuring accessibility and reproducibility of the research. Ngspice, openvaf, asm-hemt,

This thesis advances the field of cryogenic electronics by providing a robust and validated model for GaN HEMTs, facilitating their use in demanding low-temperature applications. Additionally, the use of open-source tools and workflows promotes transparency and collaboration within the research community.

1.3 *Section of This Thesis*

- In Chapter 2, I present an introduction to single-photon detectors, including an overview and the different types. I provide a detailed study of Superconducting Nanowire Single-Photon Detectors (SNSPDs), discussing their working principle, cryogenic requirements, and the design and function of readout circuits. Additionally, I examine the impact of the cryogenic environment on semiconductor devices, focusing on material behavior, device characteristics, design considerations, and cryogenic packaging and integration.

- In Chapter 3, I investigate into the physics and characteristics of High Electron Mobility Transistors (HEMTs). I include a SPICE simulation model of HEMTs, covering the DC analysis at room temperature, modifications to the ASM-HEMT model for cryogenic temperatures, and simulations of the modified HEMT at cryogenic temperatures. I also present the visualization and analysis of simulation results, focusing on key performance metrics under cryogenic conditions.

- In Chapter 4, I cover the design and integration of the SNSPD readout circuit. I discuss the modeling of SNSPD sensors and the integration of preamplifier design. I include SPICE simulations of the complete readout circuit and discuss the layout design using KLayout.

- In Chapter 5, I summarize the findings of the thesis and provide recommendations for future research. I highlight the key contributions and suggest potential areas for further investigation to advance the field of cryogenic electronics and GaN HEMT design.

This structured approach ensures a comprehensive understanding of the design and application of GaN HEMTs in cryogenic environments, integrating both theoretical and practical perspectives.

Chapter 2:
SINGLE-PHOTON DETECTION AND CRYOGENIC READOUT ELECTRONICS

2.1 *Introduction to Single-Photon Detectors*

In this section, we embark on a detailed exploration of the three principal types of photon detectors that are shaping the frontier of quantum detection technology: Single-Photon Avalanche Diodes (SPADs), Transition Edge Sensors (TES), and Superconducting Nanowire Single-Photon Detectors (SNSPDs). Each type is scrutinized for its intrinsic operational principles, strengths, and potential drawbacks. Complementing our discourse, we present Table 2.1, a comprehensive table that encapsulates the performance metrics from various studies, offering a panoramic view of the capabilities and limitations inherent to these sophisticated devices.

2.1.1 Figures of Merit for Single Photon Detectors

Photodetectors are essential for a wide range of applications, including medical imaging and telecommunication. Several performance indicators are used to evaluate their efficacy and efficiency. Here, we examine some of the most important factors that determine how well photodetectors work:

Detection Efficiency

Detection efficiency in single-photon detectors (SPD) is a pivotal measure, defined as the probability that the detector generates an output in response to a photon. Real SPDs often deviate from ideal behavior due to various factors, leading to efficiencies less than 100%. The efficiency is influenced by the wavelength of the photon and the detector's material and design. It encompasses coupling efficiency (how well photons are delivered to the detector), absorption efficiency (how effectively the detector absorbs photons) and registering probability (the likelihood of producing a signal after absorption). This overall efficiency is crucial for assessing the practical performance of SPDs in photon-counting applications.

Timing Properties

Timing properties are among the most crucial characteristics of single-photon detectors, governing the accuracy of photon detection events. The timing jitter reflects the detector's precision in recording the arrival time of a photon, and any variation here can lead to inaccuracies in temporal measurement. Dead time, on the other hand, is the period after a photon detection during which the detector is unable to sense another photon, directly limiting the count rate. Recovery time is closely related, denoting the span needed for a detector to reset and be ready for the next photon.

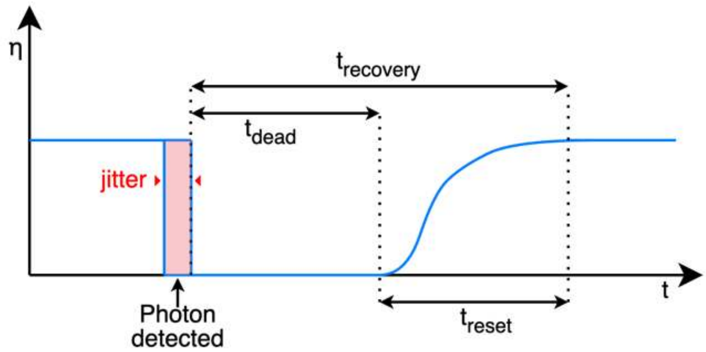

Figure 2.1: Detection efficiency as a function of time

The timing characteristics are vital for precise photon detection, as demonstrated in Figure 2.1. This figure shows the relationship between a detector's efficiency and the temporal aspects of single-photon events.

Dark Count Rate (DCR)

The dark count rate (DCR) refers to the false detections recorded by a photodetector when no light is present, effectively measuring the device's noise level. These dark counts can originate from the detector's own material properties, the way it is powered, or from environmental noise. DCR is typically expressed in Hertz or counts per second and is an essential factor in assessing a detector's performance, especially in low-light conditions. Techniques like gating, which involves activating the detector only when a photon is expected, can help reduce DCR and improve the accuracy of photon detection [45].

Photon number resolvability (PNR)

Photon number resolvability (PNR) distinguishes between detecting single or multiple photons, a critical function in quantum information applications where precise photon control is necessary. While traditional SNSPD designs offer a binary response, advanced types such as Transition Edge Sensors can indicate the quantity of photons absorbed with a resolution. This capability is crucial for secure quantum key distribution and reducing errors in quantum computing, driving research towards detectors that can accurately count individual photons.

Operational Economics and Physical Constraints

In practical applications of photodetectors, three parameters often dictate their suitability and effectiveness: cost, size, and operational temperatures. These parameters are critical as they determine not just the initial investment but also the long-term viability of the detectors in various settings. Cost considerations encompass the expense of materials and manufacturing, while size affects both the resolution capabilities and the integration into space-sensitive environments.

Superconducting detectors, like SNSPDs and TES, have an added layer of complexity with their requirement for cryogenic temperatures to maintain superconductivity. This necessity for cooling to just a few Kelvins above absolute zero imposes additional cost and size considerations due to the cryogenic systems involved. The operational temperature not only affects the detector's performance but also significantly impacts the infrastructure and energy consumption, making the trade-off between performance and practicality a vital consideration in the design and implementation of these sensitive devices.

2.1.2 Types of Single Photon Detectors

Single Photon Avalanche Photodiode (SPAD)

Single-Photon Avalanche Diodes (SPADs) are specialized photodetectors that operate on the edge of a semiconductor breakdown, where a single photon can trigger a detectable avalanche of current. A SPAD is essentially a p–n junction diode biased above its breakdown voltage VB, creating an intense electric field that can initiate a self-sustaining avalanche from a single charge carrier injected into the depletion layer [46]. The unique attribute of SPADs is their ability to produce a macroscopic current pulse in response to the detection of a photon, with a rise time that is sub-nanosecond and a corresponding current in the milliampere range [46]. This capability allows the detection of the photon's arrival time with picosecond jitter, a critical feature for applications requiring high temporal resolution.

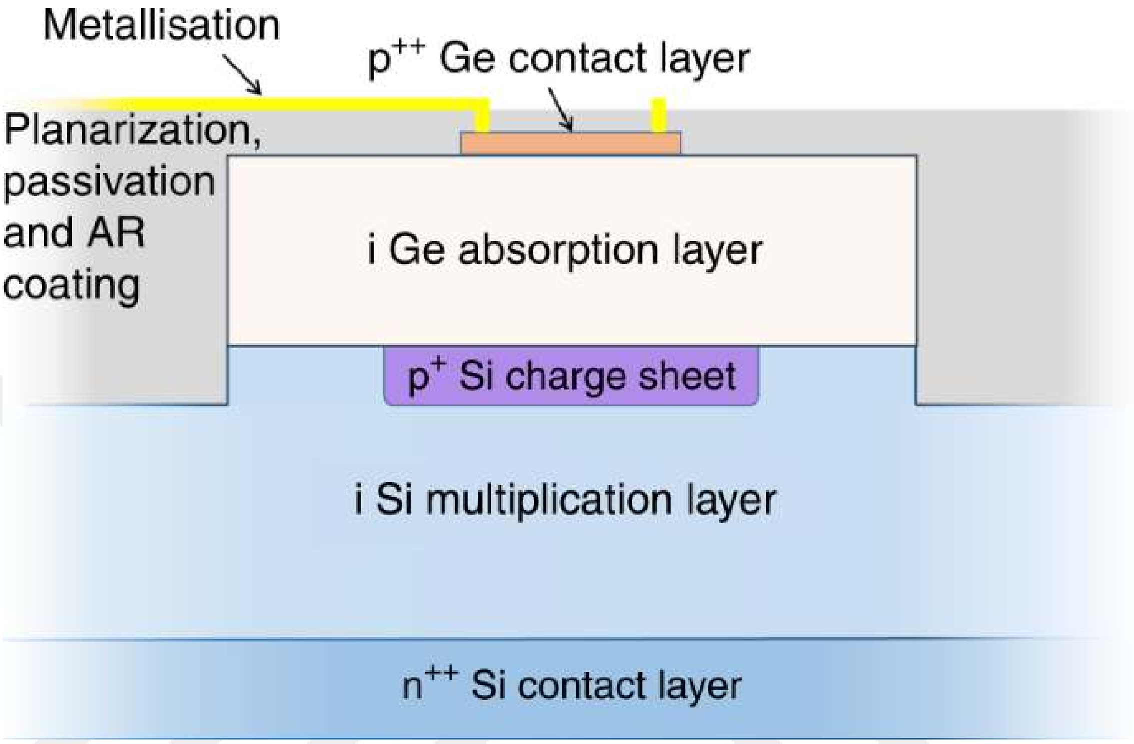

Figure 2.2: Ge-on-Si single-photon avalanche diode (SPAD) structure. [47]

In Figure 2.2, the schematic of a Ge-on-Si single-photon avalanche diode (SPAD) structure is shown. The diagram features several key layers: the metallization layer at the top, followed by a p++ Ge contact layer and an intrinsic Ge absorption layer. Beneath the Ge absorption layer is a p+ Si charge sheet, which is in turn layered over an intrinsic Si multiplication layer. At the bottom is the n++ Si contact layer. The diagram also includes a planarization, passivation, and anti-reflective (AR) coating, which helps to optimize the performance of the SPAD.

In complete darkness, a SPAD waits in an armed state until a photon is absorbed, which leads to the generation of charge carriers. These primary carriers can cause a cascade of secondary electron-hole pairs through impact ionization, discharging the diode's depletion capacitance and creating a sharp, measurable current pulse. This operational mode is referred to as Geiger mode and is a hallmark of SPAD technology [48].

SPAD's operate effectively at room temperature, which simplifies their integration into various systems without the need for complex cooling mechanisms. The advancements in SPAD technology have led to multi-pixel devices that can resolve the detection of multiple photons, broadening their applicability in quantum computing and communication. SPADs excel in detection efficiency, with certain models reaching 74% at 600 nm, a spectral range that is particularly useful for a variety of photonics applications [49]. Another variant of SPADs demonstrates 56% efficiency at 450 nm while operating at a cryogenic temperature of 78 K, which aids in reducing noise and improving signal clarity [50]. Both types of SPADs boast Photon Number Resolvability (PNR) capability, allowing for the detection and distinction between single and multiple photon events, a key feature for quantum computing and other quantum technologies. Additionally, the maximum count rate for the high-efficiency SPAD is an impressive 16 MHz [49], indicative of the device's ability to handle high-speed photon detection tasks.

Despite these advantages, SPADs do encounter certain limitations. For instance, a SPAD operating at room temperature (250 K) exhibits a dark count rate of 2000 Hz, which can introduce a significant amount of noise into the measurement process, especially in low-light conditions [49]. The cryogenic SPAD variant, while having an exceptionally low dark count rate, is limited by a maximum count rate of only 10 kHz [50], which could be restrictive for high-throughput photon counting applications. Moreover, while the maximum count rate of SPADs is generally high, allowing for the detection of a large number of photons per second, the presence of dead time can limit the effective count rate, especially in high-speed or high-flux applications.

Transition-Edge Sensor (TES)

A transition-edge sensor (TES) is an intricate micro-calorimeter employed for detecting energy through minute temperature changes. The core of a TES is an absorber coupled with a superconductive thermometer, which is characterized by a positive temperature coefficient of resistance [51]. The superconducting thermometer is delicately poised near its transition temperature, which is achieved through careful voltage-biasing. This poised state ensures that the TES operates in a region where its resistance varies significantly with even the slightest temperature variations, making it incredibly sensitive to the energy absorbed from incident photons [52].

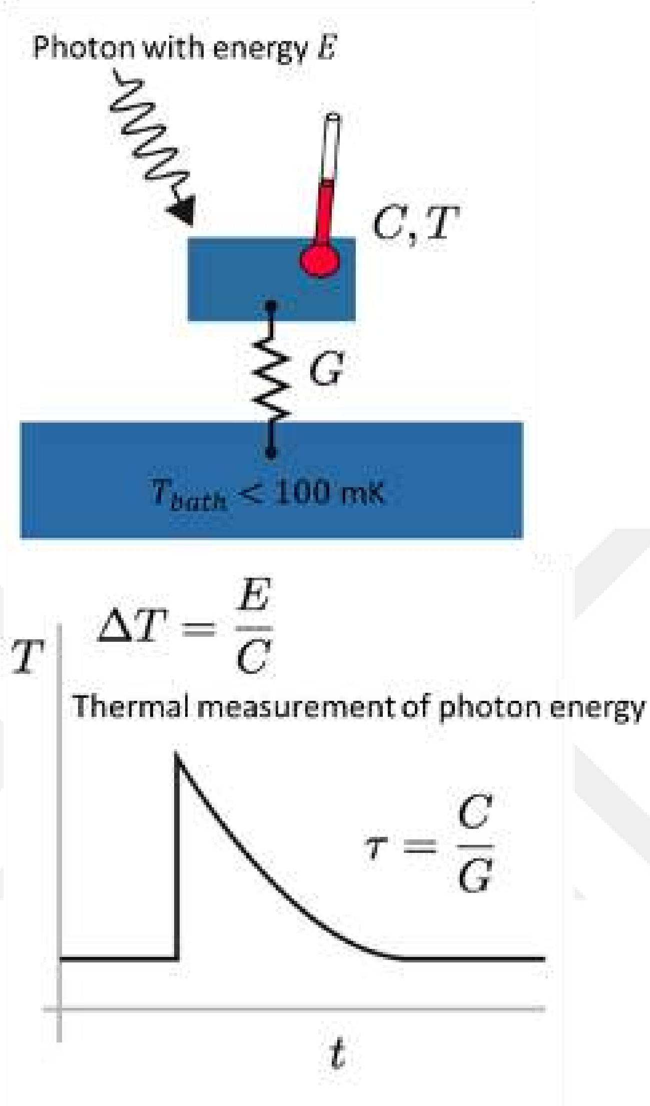

Figure 2.3: Transition Edge Sensor Schematic. [53]

The operational principle of a TES revolves around the fundamental physics of superconductivity. The superconducting state is defined by an energy gap which dictates the presence of Cooper pairs—paired electrons that behave as superconducting charge carriers. These pairs exist due to a weak attractive interaction, often facilitated by phonon exchange [54]. When a photon with sufficient energy interacts with the TES, it disrupts these Cooper pairs, generating quasiparticles. While in conventional detectors like STJ or KIDs, the count of these quasiparticles is used as a measure of photon detection, a TES utilizes a different approach. It measures the collective effect of these quasiparticles as a change in temperature, thanks to the sensitive thermometer embedded within. This temperature change, a result of the Cooper pairs breaking, provides an accurate measure of the energy of the absorbed photon [55].

In Figure 2.3, the schematic of the transition edge sensor (TES) is illustrated. The TES absorbs a photon with energy E, leading to a temperature increase ΔT in the sensor. The TES, characterized by its heat capacity C and temperature T, is thermally connected to a heat bath at a lower temperature via a thermal conductance G. The temperature increase ΔT is given by the equation $\Delta T = EC$. The resulting temperature decay over time t follows the thermal relaxation time constant $\tau = CG$.

Transition Edge Sensors (TES) are renowned for their exceptional photon number resolvability and high detection efficiency, with some variants exhibiting up to 95% at 1550 nm wavelengths, making them highly reliable for near-infrared photon detection [56]. They operate at millikelvin temperatures (100mK – 200mK), which, while demanding in terms of cooling requirements, provide a low-noise environment crucial for their operation. Moreover, the dark count rate is very low, sometimes reaching the negligible range, which greatly enhances the signal-to-noise ratio of these detectors.

Despite their remarkable sensitivity and precision, TES devices are not without their limitations. The main limitation of TES detectors is their need for ultra-low operational temperatures, necessitating complex and costly cryogenic systems. While the dark count rate is minimal, the operational economics related to the cooling infrastructure could be a significant barrier, especially for long-term or widespread application. Additionally, the intrinsic characteristics of TES, such as longer recovery times and timing jitter within the nanosecond range, inherently limit their maximum count rate. These factors collectively render TES less suitable for applications requiring rapid photon detection sequences, as they cannot reliably sustain the high-count rates that such processes demand.

Superconductor Nanowire Single Photon Detector (SNSPD)

A superconducting nanowire single-photon detector (SNSPD) operates based on the unique physical properties of a superconducting nanowire, which can be in one of three states: superconducting, normal, and resistive. Initially, in the superconducting state, the nanowire demonstrates zero electrical resistance and functions similarly to an inductor with kinetic inductance L_k [57]. This state persists until the device current (I_d) increases to a critical value known as the switching current (I_{sw}). The I_{sw} is sensitive to temperature, decreasing as temperature rises [57]. The transition from the superconducting to the normal state occurs when I_d reaches I_{sw}. This can happen either by increasing I_D through the bias current (I_b) or due to the absorption of a photon. For a photon to trigger this transition, its energy must exceed the superconducting energy gap ($h\omega \gg 2\Delta$) [58]. The energy imparted by the photon increases the local temperature, thereby reducing I_{sw} at that point and leading to the formation of a resistive hotspot. This hotspot, with resistance typically ranging from 1 to 10 kΩ, is contingent on the nanowire's dimensions and material composition [57][58].

As this hotspot forms, a voltage signal is generated across the nanowire, marking the transition to the resistive state. The dynamics of the hotspot involve a competition between Joule heating, which drives its expansion, and a cooling process where electrons lose energy through electron-phonon scattering. If cooling is more effective than heating, the hotspot dissipates, returning the nanowire to its superconducting state [58].

The final resistive state, where the entire nanowire becomes resistive and displays ohmic behavior, is not typically utilized in single-photon detection applications, thus is not a primary focus for SNSPDs.

Superconducting Nanowire Single-Photon Detectors (SNSPDs) stand at the forefront of high-speed photon timing applications, thanks to their exceptional timing resolution. Certain models can achieve timing jitter as minuscule as 30 picoseconds [59], which is essential for capturing the rapid succession of photons. Additionally, these detectors are capable of handling extensive photon fluxes, with some variants supporting maximum count rates that soar up to 1 GHz [59][60]. While boasting good timing parameters, they also maintain relatively high detection efficiencies, like 57% with low dark count rates at 1550 nm within a cavity [59].

Despite their operational advantages, SNSPDs are not without their challenges. While the operational temperature for SNSPDs is higher than TES (1.5 K to 4 K), it still necessitates cooling equipment, which could impact the size and cost. Additionally, SNSPDs typically lack intrinsic Photon Number Resolvability, limiting their use in quantifying photon numbers.

Table 2.1: Comprehensive Overview of Single-Photon Detector Specifications from Literature, PNR: Photon Number Resolvability

Detector Type	Operation Temperature	Detection Efficiency (% @ λ, nm)	Timing Jitter	Dark Count Rate	PNR Capability	Max Count Rate	Ref.
Si SPAD	250K	74 @ 600	-	2000 Hz	Yes	16 MHz	[49]
Si SPAD	78K	56 @ 450	-	0.001 Hz	Yes	10 kHz	[50]
TES	100mK – 200mK	95 @ 1550	-	Negligible	Yes	100 kHz	[15]
TES	100mK	95 @ 1556	100 ns	Negligible	Yes	100 kHz	[61]
InGaAs SPAD	243K	10 @ 1550	55 ps	16 kHz	No	100 MHz	[62]
TES	110mK	88 @ 1550	-	400 Hz	Yes	-	[63]
Parallel SNSPD	2K	2 @ 1300	50 ps	0.15 Hz	Yes	1 GHz	[60]
SNSPD	1.5K	57 @ 1550	30 ps	-	No	1 GHz	[59]
TES	100mK	50 @ 1550	100 ns	3 Hz	Yes	100 kHz	[64]
SNSPD	3K	2 @ 1550	60 ps	1 kHz	No	-	[65]
SNSPD	< 4K	>90 @ 1550	150 ps	1 Hz	No	25 MHz	[66]

2.2 *Detailed Study of SNSPDs*

2.2.1 *Working Principle and Physics*

The working principle of superconducting nanowire single-photon detectors (SNSPDs) is fundamentally based on the transition from the superconducting state to the resistive state, triggered by the absorption of an incoming photon.

Superconductivity is a quantum mechanical phenomenon where, below a critical temperature, certain materials exhibit zero electrical resistance and expel magnetic fields. This state is maintained by Cooper pairs, which are pairs of electrons bound together at low temperatures that move through the lattice without scattering. The absence of scattering allows for the free flow of electric current with no energy loss, which is a crucial property for the operation of SNSPDs.

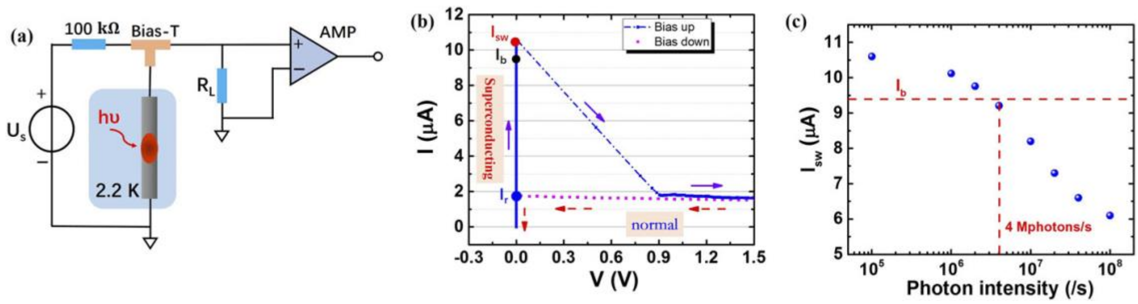

Figure 2.4: (a) Schematic of quasi-constant-current-bias circuit for SNSPD. (b) Current-voltage curve of SNSPD without light. Solid arrows indicate the up sweep curve from 0 to 1.5 V. Dash arrows indicate the down sweep from 1.5 to 0 V. [67]

In the cryogenic environment, the superconducting nanowire in an SNSPD is typically biased with a constant current source. As illustrated in Figure 2.4 (a), which shows an example setup, the system includes a bias resistor, a bias-tee, a load resistor R_L, and an amplifier. When a photon strikes the nanowire, its energy is absorbed, causing a localized disruption in the superconducting state and resulting in a temporary increase in resistance. This increase in resistance generates a voltage pulse across the nanowire. The pulse is then transmitted through the load resistor R_L to the amplifier, which amplifies the signal for further processing. After the pulse is generated, the nanowire undergoes a recovery process where the resistive region cools down, allowing Cooper pairs to reform and the superconducting state to be restored. Once the nanowire has fully recovered, it is ready to detect another photon.

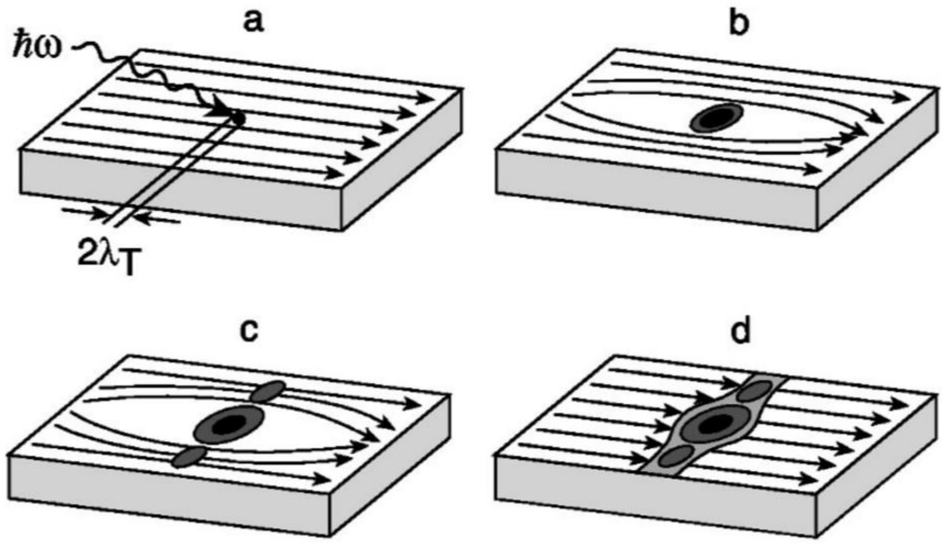

Figure 2.5: Schematics of the supercurrent-assisted hotspot formation mechanism in an ultrathin and narrow superconducting strip, kept at temperature far below T_C are shown. The arrows indicate direction of the supercurrent flow. [58]

The changes in the superconducting nanowire upon photon absorption can be explained by the following physical phenomena.

Hotspot Creation

When a photon strikes the superconducting nanowire, its energy is absorbed, causing a localized disruption in the superconducting state. The energy of the photon must be greater than the superconducting gap energy, which is the energy required to break Cooper pairs. Upon absorption, the photon's energy is transferred to the electrons in the nanowire, breaking Cooper pairs and creating quasiparticles (unpaired electrons). This localized energy deposition leads to the creation of a hotspot, as illustrated in Figure 2.5(a), an area where the temperature is temporarily elevated. This results in a localized region where the superconducting state is disrupted, and the resistance increases. The hotspot is essentially a small, temporary region of normal (non-superconducting) state within the superconducting nanowire.

Supercurrent Redistribution:

The formation of a hotspot forces the supercurrent to redistribute around the non-superconducting region. As shown in Figure 2.5(b), the current density increases in the remaining superconducting areas due to the fixed width of the nanowire. As the hotspot grows, as depicted in Figure 2.5(c), Joule heating causes further disruption of superconductivity, resulting in a larger resistive region. This redistribution of supercurrent and the subsequent formation of a larger resistive barrier occur if the current density exceeds the critical current density (I_c) of the superconducting material.

Voltage Pulse Generation:

The appearance of the resistive region results in a measurable voltage pulse across the nanowire since constant current source is applied to the nanowire. The amplitude of this pulse is directly proportional to the size of the resistive region and the current passing through the nanowire. This voltage pulse can be detected by readout electronics, which indicate the arrival of a photon. Figure 2.5(d) illustrates the expansion of the resistive region and the subsequent voltage pulse generation.

Recovery Process

After the initial creation of the hotspot and the resulting voltage pulse, the nanowire begins to cool down, allowing the normal (non-superconducting) region to shrink. The quasiparticles recombine to form Cooper pairs, restoring superconductivity in the affected region. This recovery process is rapid, typically occurring on a timescale of a few picoseconds to nanoseconds, allowing the detector to reset and be ready for another photon detection event.

2.2.2 Design and Function of Readout Circuits

Readout electronics are critical for the performance of Superconducting Nanowire Single-Photon Detectors, as they influence key characteristics such as timing resolution (jitter), reset time, and maximum count rate. Effective readout circuits are essential for optimizing these parameters and ensuring the detector's overall efficiency and reliability.

One of the main challenges in readout circuit design is achieving low-noise amplification. This is crucial for improving the signal-to-noise ratio and reducing timing jitter, both of which are vital for accurate photon detection [68]. Additionally, a high bandwidth is necessary to capture the fast rise time of SNSPD signals accurately, ensuring that the detector can respond quickly to incoming photons [68]. Another significant challenge is maintaining high count rates while minimizing power consumption, particularly for large SNSPD arrays [28].

Cryogenic amplifiers play a significant role in readout circuits for SNSPDs. These amplifiers offer advantages such as reduced noise and closer proximity to the detector, which enables better impedance matching and overall improved performance [28]. Moreover, to address the issue of gain variation with temperature in cryogenic environments, temperature-insensitive designs have been introduced. These designs ensure consistent performance across a range of operating conditions.

Scalability and integration are also crucial considerations in the design of readout circuits for SNSPDs. Scaling readout circuits for large SNSPD arrays presents unique challenges. One approach to managing scalability involves balancing the trade-offs between on-chip digitization and analog multiplexing [69]. Additionally, low power consumption is vital for enabling multi-channel readout systems, which are essential for scalable and efficient detector arrays [28].

In conclusion, the design of readout circuits for SNSPDs involves addressing several key challenges, including low-noise amplification, high bandwidth, and power consumption. Cryogenic amplifiers and scalable integration strategies play crucial roles in overcoming these challenges and enhancing the overall performance of SNSPDs. By focusing on these aspects, we can develop more efficient and reliable readout circuits that meet the demands of various applications in quantum communication and imaging.

Chapter 3:
HIGH ELECTRON MOBILITY TRANSISTOR DESIGN FOR CRYOGENIC ENVIRONMENTS

High Electron Mobility Transistors (HEMTs) are essential components in modern electronics, particularly in high-frequency applications. The primary advantage of HEMTs over traditional field-effect transistors (FETs) lies in their heterostructure, which enables high electron mobility due to the formation of a two-dimensional electron gas (2DEG).

This chapter first provides an overview of the physics and characteristics of High Electron Mobility Transistors (HEMTs), focusing on their key development milestones, the physics of Gallium Nitride (GaN) based HEMT devices and related concepts, and the effects of cryogenic temperatures on GaN based HEMT devices. Then, we investigate the structural design of a GaN HEMT for cryogenic preamplifiers and use Ngspice simulations to identify the device behavior under different V_{GS} bias voltages at room temperature for DC analysis and cryogenic temperatures. For SNSPD and cryogenic preamplifier devices, high-frequency behavior must be understood. We studied and present here the frequency-dependent drain voltage at 4.2 K, which is a common operating temperature for the devices. For future fabrication and testing, we prepared a lithography mask layout design using KLayout for a GaN HEMT device for a cryogenic preamplifier. These steps could pave the way for the future implementations of cryogenic GaN HEMT preamplifiers for quantum information processing.

3.1 Key Milestones in the Development of HEMT Devices

The High Electron Mobility Transistor (HEMT) has seen significant advancements since its inception. In 1975, Takashi Mimura observed and explained the structural phenomena of HEMTs, laying the groundwork for their future development [70]. Mimura conceptualized HEMTs while working on GaAs MOSFETs, inspired by the modulation-doped heterojunction superlattice developed by Dingle et al., which demonstrated high electron mobility due to the separation of electrons and their donor impurities [71].

In 1994, Khan et al. successfully created a two-dimensional electron gas (2DEG) using a GaN/AlGaN heterostructure, significantly advancing HEMTs for high-power and high-frequency applications [72]. This achievement marked a significant milestone in the application of HEMTs to wide bandgap materials, particularly enhancing their performance in demanding environments.

In 2004, Eudyna Corporation demonstrated a depletion-mode GaN HEMT for RF applications, and in 2005, Nitronex Corporation announced their GaN-on-Si HEMTs for similar applications. The first enhancement-mode GaN devices were developed by EPC in 2009 [73].

In 2014, the cryogenic performance of HEMT amplifiers operating above 300 GHz was presented for the first time, demonstrating a gain of 16 dB at 312 GHz by cooling the device to 28 K [74]. This highlighted the advancements in HEMT technology and their suitability for extreme environments such as cryogenic temperatures.

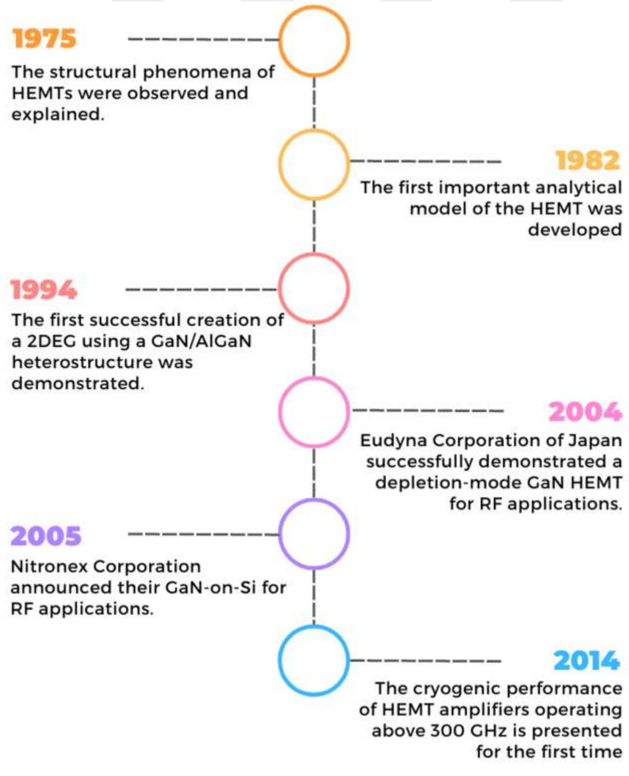

Figure 3.1: Timeline of Key Milestones in the Development of High Electron Mobility Transistors (HEMTs)

The development of analytical modeling for HEMTs has been crucial in advancing their design and understanding. Analytical models provide a framework for predicting and optimizing the behavior of HEMTs under various conditions. They are essential for understanding the charge transport mechanisms and for the design of more efficient and high-performance devices.

In 1982, Delagebeaudeuf and Linh developed the first analytical model of HEMTs, which was crucial for understanding their C-V and I-V characteristics [75]. However, it was limited by the assumption of a bias-independent Fermi level [76]. This limitation was later addressed by An-Jui et al. with a more accurate nonlinear charge control model [77].

In this model, the nonlinear dependence of the sheet carrier concentration of the two-dimensional electron gas (2DEG) has been taken into account in the quasi-triangular potential quantum well of the HEMT. This consideration helped capture a bias-dependent effective offset distance of the 2DEF from the heterointerface. This nonlinear solution helped identify the bias dependence of the Fermi potential.

The significant milestones in the history of HEMT development are illustrated in Figure 3.1. These key dates highlight the progressive advancements and the pivotal research contributions that have shaped the current state of HEMT technology.

3.2 Physics of GaN Based HEMT Devices and Related Concepts

High Electron Mobility Transistors (HEMTs) leverage advanced semiconductor physics to achieve superior performance in high-frequency applications [78][79]. The key to their exceptional functionality lies in the unique physics of their heterostructures, which include concepts such as heterojunctions, two-dimensional electron gas (2DEG), and polarization effects. This section explores these critical aspects in detail.

3.2.1 Heterojunction Formation

A heterojunction is formed when two semiconductor materials with different bandgaps are joined together. In GaN-based HEMTs, the heterojunction typically consists of a layer of AlGaN (Aluminum Gallium Nitride) and a layer of GaN. The difference in bandgap and electron affinity between these materials leads to the creation of a two-dimensional electron gas (2DEG) at the interface. This 2DEG provides high electron mobility because the electrons are confined in a potential well, minimizing scattering from impurities and lattice vibrations [80].

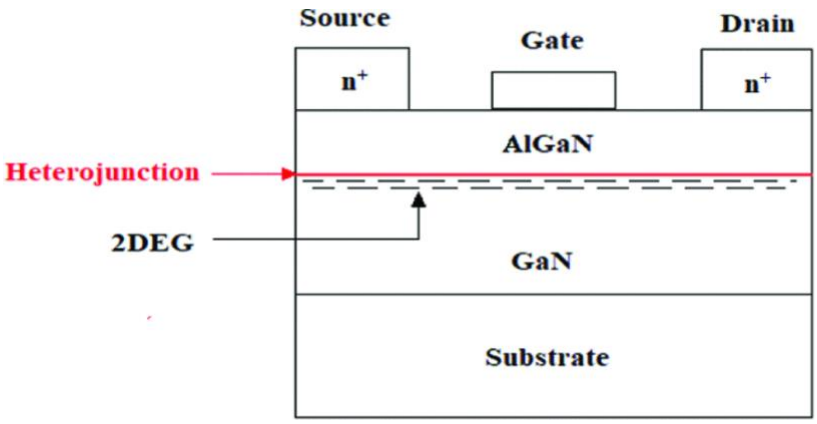

Figure 3.2: Structure of AlGaN/GaN HEMT © 2019 IEEE. Reprinted, with permission, from J. C. Choton, A. Begum and J. K. Saha, "Design and Characterization of 2DEG Structure of a Gallium Nitride HEMT," 2019 International Conference on Robotics,Electrical and Signal Processing Techniques (ICREST), Dhaka, Bangladesh, 2019, pp. 486-489

In Figure 3.2, the structure of a GaN-based HEMT is provided, illustrating the heterojunction formation. The figure shows how the AlGaN layer is grown on top of the GaN layer, creating a heterojunction at their interface. The resulting difference in bandgap energies between AlGaN and GaN leads to the accumulation of free electrons at the interface, forming the 2DEG. This electron gas is confined to a narrow region, providing high mobility and enabling efficient operation of the HEMT at high frequencies.

3.2.2 Two-Dimensional Electron Gas (2DEG)

The Two-Dimensional Electron Gas (2DEG) is a crucial aspect of GaN-based High Electron Mobility Transistors (HEMTs), contributing significantly to their exceptional performance. The 2DEG forms at the heterojunction interface between the AlGaN barrier layer and the GaN channel layer due to the unique polarization properties of III-nitride materials and the band structure differences between AlGaN and GaN.

As depicted in Figure 3.1, the 2DEG is formed at the interface of the AlGaN and GaN layers. This process starts with the inherent polarization of the III-nitride materials, which creates a conduction path at the interface of the upper (AlGaN) and lower (GaN) layers. The polarization-induced charges at the interface result in a net positive charge due to the dissimilarity between the AlGaN and GaN layers. Consequently, the conduction band bends downwards near the interface, causing electrons to accumulate in the potential well formed at this junction. The contacts are Ohmic in the GaN HEMT devices.

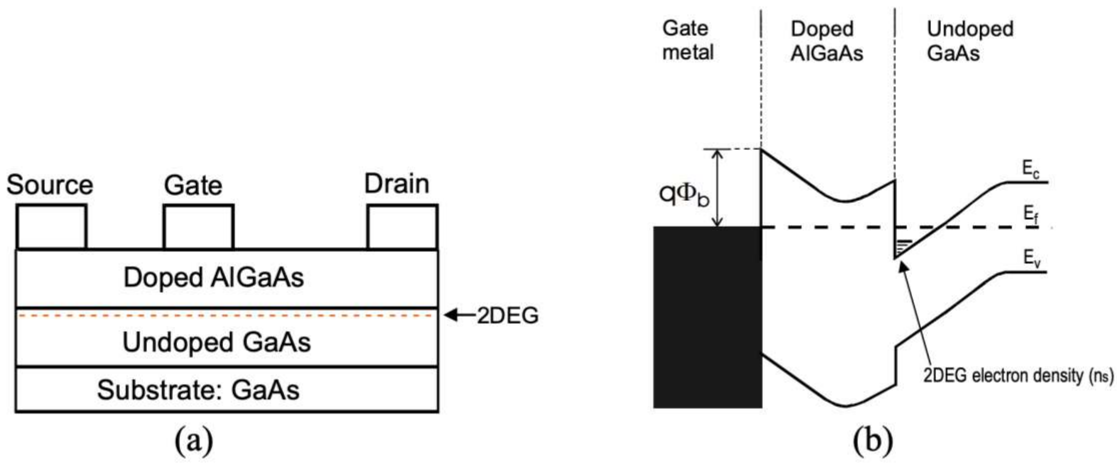

Figure 3.3: Simplified AlGaAs/GaAs HEMT structure, (b) corresponding band diagram. [104]

These electrons are confined in a narrow triangular-shaped potential well at the interface, whose solutions are already known as Airy functions [105], as illustrated by the yellow region in Figure 3.3. This confinement restricts their movement perpendicular to the interface while allowing them to move as a free particle parallel to the interface. The electrons trapped in this region form the 2DEG, which is characterized by high carrier density and mobility [106].

The electrons confined in this 2DEG exhibit several advantageous properties:

- **High Carrier Density:** The 2DEG has a very high carrier density because the potential well attracts and confines a large number of electrons at the interface. This high carrier density improves the overall conductivity of the channel, enabling the HEMT to handle high current densities efficiently [107].

- **High Mobility:** The confinement of electrons in the potential well minimizes scattering from impurities and lattice vibrations, leading to exceptionally high electron mobility. High mobility is crucial for the high-speed performance of GaN HEMTs, as it allows for faster electron transit times and improved transconductance [108].

- **Superior Performance Characteristics:** The high mobility and density of the 2DEG contribute to the superior performance characteristics of GaN HEMTs, including high transconductance, high current density, and low noise figures. High transconductance enables efficient signal amplification, high current density supports power applications, and low noise figures are essential for high-frequency and low-noise applications [109][110][111].

- **Reduced Parasitic Effects:** The formation of the 2DEG minimizes parasitic resistances and capacitances in the device. This reduction is crucial for maintaining high-frequency performance and ensuring that the HEMT operates efficiently in RF and microwave applications [112][113].

- **Increased bandwidth and dynamic range:** A natural consequence of reduced parasitic effects is the increase in signal-to-noise ratio of the GaN HEMT devices. This increase in the SNR allows for broader bandwidth operations [114].

3.2.3 Polarization Effects

Polarization effects play a crucial role in the operation and performance of High Electron Mobility Transistors (HEMTs), particularly those based on III-nitride materials like Gallium Nitride (GaN) and Aluminum Gallium Nitride (AlGaN). These effects arise from the unique crystal structure and inherent properties of these materials, significantly influencing the behavior of charge carriers at the heterojunction interface. Polarization in HEMTs can be categorized into two primary types: Spontaneous Polarization (P_{SP}) and Piezoelectric Polarization (P_{PE}). Both types contribute to the formation and enhancement of the two-dimensional electron gas (2DEG), which is essential for the high electron mobility that characterizes HEMT devices.

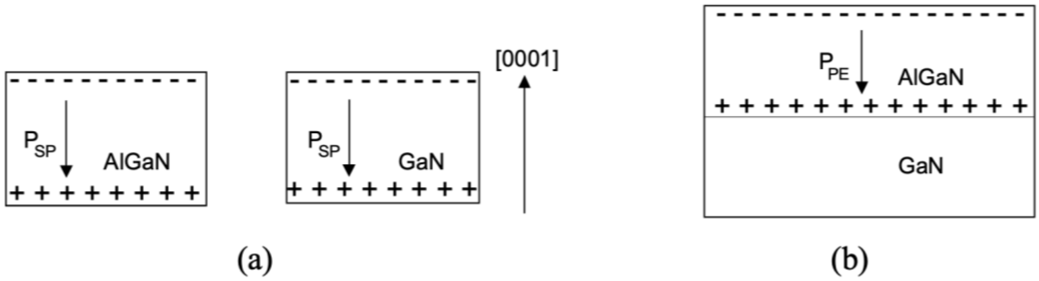

Figure 3.4: Electric field and sheet charges present (a) due to only spontaneous polarization in GaN and AlGaN crystals; and (b) due to only piezoelectric polarization in a AlGaN layer.

Spontaneous Polarization (PSP)

Spontaneous polarization is an intrinsic property of III-nitride materials resulting from their wurtzite crystal structure, which lacks inversion symmetry. This structural asymmetry causes a natural alignment of electric dipoles within the crystal lattice, leading to a net polarization even in the absence of external stress or electric fields. In GaN and AlGaN, the spontaneous polarization creates a built-in electric field that can significantly affect the distribution of charge carriers at the heterojunction interface [81].

As shown in Figure 3.4(a), the difference in spontaneous polarization between the AlGaN and GaN layers induces a fixed positive charge at the AlGaN/GaN interface. This positive charge attracts electrons from the AlGaN layer, leading to the formation of a high-density two-dimensional electron gas (2DEG) in the GaN layer. This phenomenon is a key factor in enhancing the conductivity of the GaN layer, as the electrons are attracted to the positive charge at the interface, resulting in the creation of the 2DEG.

Piezoelectric Polarization (PPE)

Piezoelectric polarization is induced by mechanical strain resulting from lattice mismatches between different semiconductor layers in the HEMT structure. When a layer of AlGaN is grown on GaN, the difference in their lattice constants causes strain in the AlGaN layer. This strain generates piezoelectric polarization charges due to the piezoelectric nature of the III-nitride materials.

As depicted in Figure 3.4(b), the piezoelectric polarization (P_{PE}) in the strained AlGaN layer creates additional polarization charges at the AlGaN/GaN interface, further enhancing the 2DEG density [82].

The combination of spontaneous and piezoelectric polarization effects leads to a higher concentration of mobile electrons in the 2DEG, significantly improving the HEMT's performance in terms of transconductance, current density, and frequency response.

The interplay between spontaneous and piezoelectric polarization is crucial for the design and optimization of GaN-based HEMTs. By carefully controlling the composition and thickness of the AlGaN layer, engineers can optimize the polarization effects to achieve the desired electrical characteristics, making GaN HEMTs suitable for high-frequency applications.

3.3 *Effects of Cryogenic Temperatures on GaN based HEMT Devices*

The performance of HEMTs, particularly GaN-based HEMTs, can be significantly affected by operating temperatures. Notably, their thermal and flicker noise significantly decrease at cryogenic temperatures, extending their utility to quantum computing and deep space exploration through low-noise amplifiers. These temperature-dependent improvements make GaN-based HEMTs highly advantageous for applications requiring high precision and low noise in extreme environments [83].

Compared to traditional silicon-based devices, GaN HEMTs offer superior thermal capacitance, breakdown voltage, and saturated drift velocity, making them well-suited for operation in harsh conditions. The comparison between silicon (Si) and gallium nitride (GaN) in Table 3.1 highlights the significant advantages of GaN for cryogenic electronic devices. GaN's wider bandgap (3.44 eV) compared to Si (1.1 eV) allows for improved sensitivity and time resolution, making it suitable high-frequency applications. Additionally, GaN's higher electron mobility (2000 $cm^2/V \cdot s$) compared to Si (1450 $cm^2/V \cdot s$) results in higher conductivity and lower resistance, which in turn leads to lower power dissipation and enhanced efficiency. The thermal conductivity κ of the GaN is lower than Si. The implication of it is that GaN has lower power dissipation. These characteristics make GaN HEMTs excellent candidates for operation at cryogenic temperatures.

Table 3.1: Comparison of Material Properties of Si and GaN

Properties	Unit	Si	GaN	Ref.
Bandgap	E_g [eV]	1.1	3.44	[86]
Thermal conductivity	κ [W/cm·K]	1.5	1.3	[86]
Mobility	μ [cm^2/V ·s]	1450	2000	[84][85]

At cryogenic temperatures, several changes occur that can enhance the performance of GaN HEMT devices:

- **Improved DC Performance:** At cryogenic temperatures, electron mobility in GaN HEMTs increases dramatically. For instance, in InAlN/AlN/GaN HEMTs, electron mobility can rise from 1600 cm^2/Vs at room temperature to 16,000 cm^2/Vs at 5 K [87]. This increase in mobility is primarily due to the reduction in phonon scattering at lower temperatures. As a result, the on-resistance of the device also decreases significantly [88], enhancing the overall DC performance [89][90].

- **Improved RF Performance:** The RF performance of GaN HEMTs is also notably improved at cryogenic temperatures. Studies have shown that as the temperature decreases, there are increases in maximum available power gain, short-circuit current gain, and open-circuit voltage gain [91]. Additionally, improvements in drain current, transconductance, and cutoff frequency are observed, which are critical parameters for high-frequency applications [92].

- **Improved Noise Performance:** Noise characteristics of GaN HEMTs benefit greatly from cryogenic operation. At temperatures around 10 K, there is a significant reduction in the noise temperature of the devices [93]. This reduction is crucial for applications requiring low-noise performance, such as in communication systems and sensitive measurement equipment.

- **Reduced Switching Losses:** GaN power devices also exhibit reduced switching losses at cryogenic temperatures. The increased carrier mobility at lower temperatures leads to a notable reduction in conduction losses, thereby improving the efficiency of the devices [88]. This improvement is particularly beneficial for power electronics applications where high efficiency is critical.

In conclusion, operating GaN HEMT devices at cryogenic temperatures significantly enhances their performance. These improvements include better DC and RF characteristics, reduced noise, and lower switching losses. Such enhancements make GaN HEMT technology highly suitable for advanced applications in space exploration, satellite communication, and cryogenic power electronics.

3.4 Structural Design of GaN HEMT for Cryogenic Preamplifier

The design and characteristics of the GaN HEMT device used in Zeng et al. [94] were selected for integration into a cryogenic preamplifier due to their promising experimental results.

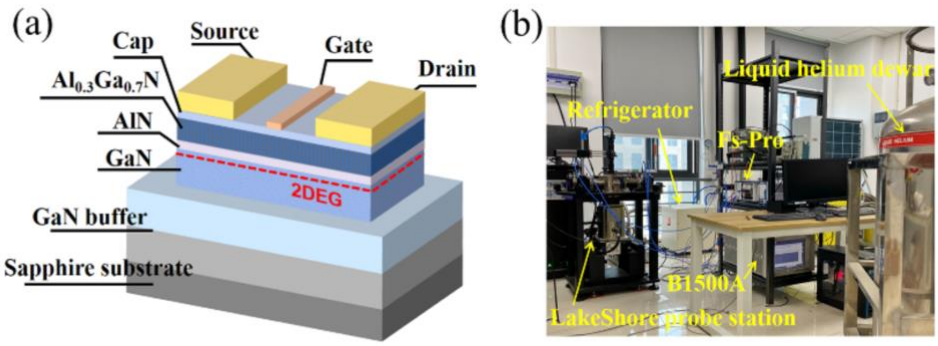

Figure 3.5: (a) Schematic diagram of GaN-based HEMT. (b) The test platform for temperature-dependent DC and LFN characterizations, including the probe station, semiconductor analyzers, and liquid helium dewar. [94]

As illustrated in Figure 3.5(a), the schematic diagram of the GaN-based HEMT shows the layered structure comprising a sapphire substrate, an unintentionally doped GaN buffer layer, a 1 nm AlN spacer layer, a 20 nm $Al_{0.3}Ga_{0.7}N$ barrier layer, and a 3 nm GaN cap layer. The gate contact is made of Ni/Au, while the source/drain contacts consist of Ti/Al/Ni/Au.

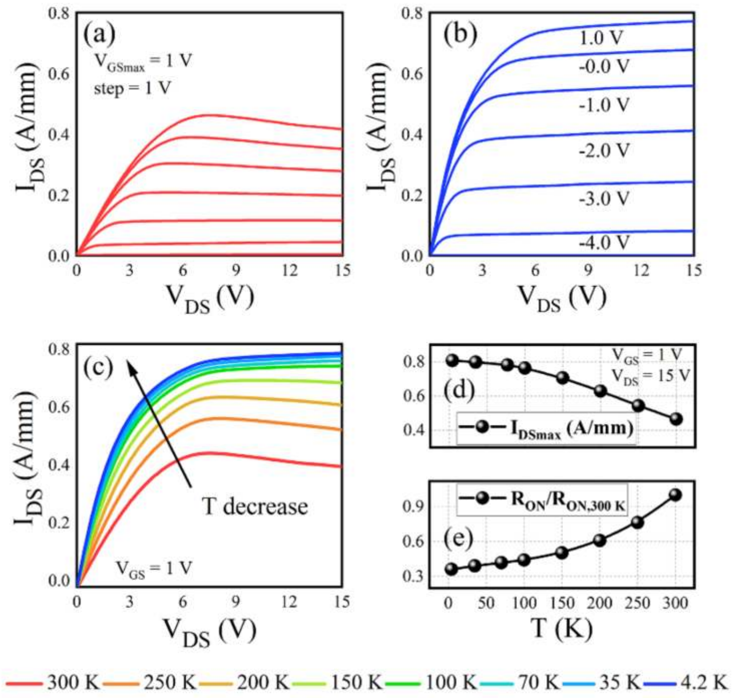

Figure 3.6: DC characteristics of the DUT under various T: output characteristics at (a) 300 K and (b) 4.2 K. (c) Comparison of the output curves at V_{GS} = 1 V from 300 K to 4.2 K. Extracted (d) $I_{DS,max}$ and (e) RON as a function of T from the output curves. [94]

The experimental results for the GaN HEMT device under different temperature conditions are illustrated in Figure 3.6. Figure 3.6(a) shows the output characteristics of the GaN HEMT at room temperature (300 K). This plot illustrates the drain current (I_{DS}) as a function of the drain-source voltage (V_{DS}) for different gate-source voltages (V_{GS}), demonstrating the typical behavior of the device at room temperature. When the temperature is lowered to cryogenic levels, as shown in Figure 3.6(b), the output characteristics change significantly. At 4.2 K, the device shows a marked increase in drain current, highlighting the enhanced performance at these low temperatures.

Figure 3.6 (c) compares the output curves at a gate-source voltage (V_{GS}) of 1 V across a range of temperatures from 300 K to 4.2 K. The plot uses a color gradient to indicate temperature, with red representing 300 K and blue representing 4.2 K. This comparison clearly shows the improvement in drain current and reduction in on-resistance as the temperature decreases, emphasizing the benefits of operating GaN HEMTs at cryogenic temperatures.

To quantify these improvements, Figure 3.6(d) presents the extracted maximum drain current ($I_{DS,max}$) as a function of temperature. The graph indicates a 75% increase in $I_{DS,max}$, rising from 461 mA/mm at 300 K to 808 mA/mm at 4.2 K. This significant enhancement in drain current at lower temperatures demonstrates the superior performance of the device in cryogenic environments. Furthermore, Figure 3.6**(e)** shows the extracted on-resistance (R_{ON}) as a function of temperature. The plot reveals a decrease in R_{ON} with decreasing temperature, with notable changes observed below 100 K. This reduction in on-resistance contributes to the overall improvement in the device's efficiency at cryogenic temperatures.

Collectively, these figures illustrate the substantial enhancements in the electrical characteristics of the GaN HEMT device when operated at cryogenic temperatures. The improvements in maximum drain current and on-resistance make GaN HEMTs highly suitable for low-temperature applications such as cryogenic preamplifiers.

To validate the suitability of the GaN HEMT device for cryogenic preamplifier applications, we conducted SPICE simulations and compared the results with experimental data.

3.5 SPICE Simulation of GaN HEMT Device

To simulate the operational performance of the GaN HEMT device, SPICE simulations were carried out using ngspice, an open-source simulation program. Ngspice is a highly versatile and widely used SPICE simulator capable of simulating electrical and electronic circuits. It can handle circuits with various components, including JFETs, bipolar and MOS transistors, passive elements (R, L, C), diodes, transmission lines, and even digital circuits. Additionally, ngspice supports mixed-signal circuits, which combine analog and digital components in a single simulation environment.

A notable feature of ngspice is its integration with Verilog-A compact device models via the OSDI/OpenVAF interface. This integration allows the use of modern models such as PSP or FinFET BSIM-CMG without needing to program on the ngspice side. Verilog-A has become the de facto standard for developing and distributing compact models due to its simulator-independent and standardized language. Verilog-A compilers translate these models into machine code, enabling simulators to use them without manual implementation.

Verilog-A enhances model development and customization by allowing quick modifications to the model equations. It supports the implementation of behavioral or data-driven models and ensures portability between simulators for both models and process design kits (PDKs).

The OSDI format enables the loading of compiled Verilog-A compact device models at runtime. OpenVAF, a Verilog-A compiler, is essential for compiling these models for use in circuit simulators. OpenVAF aims to provide high-quality, standard-compliant compilation with features like fast compile times, an intuitive user interface, and efficient simulation performance.

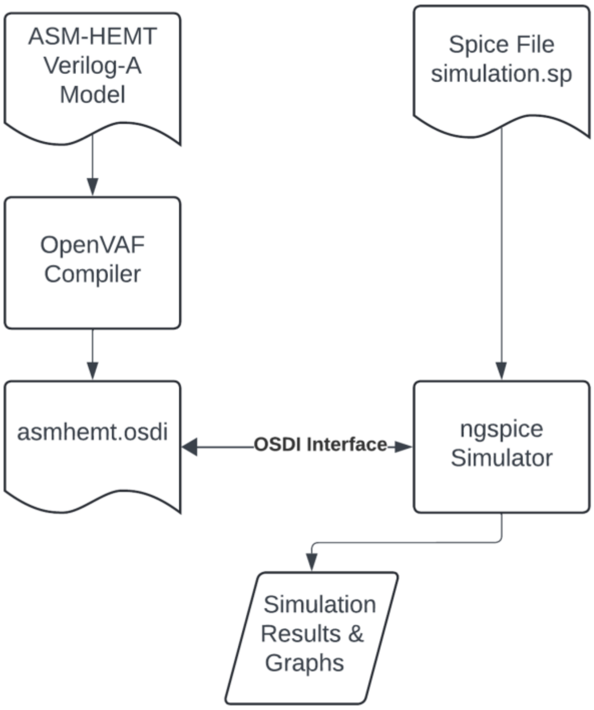

Figure 3.7: Steps Involved in Simulating GaN HEMT with Ngspice

In this work, the ASM-HEMT model [95] is used for the GaN HEMT device simulation. The ASM-HEMT model is a physical, surface-potential-based model that is computationally efficient due to its fully analytical nature. It includes various real device effects such as velocity saturation, access region resistance, DIBL, temperature dependence, and models for gate current and noise. The ASM-HEMT model, coded in Verilog-A, enables easy integration and modification within simulation environments.

The model offers analytical solutions for surface potential and intrinsic charges, which form the foundation for accurate drain current calculations [96]. It includes critical effects like velocity saturation, mobility degradation, short-channel effects such as DIBL, and self-heating. Additionally, the model features a comprehensive charge model for all terminal charges, adhering to charge conservation principles to enhance simulation convergence [96]. Furthermore, the ASM-HEMT model includes gate current models using diode-based formulations and accounts for both thermal and flicker noise, which are crucial for RF and low-noise applications. It also simulates trapping effects, such as drain-lag and gate-lag, using RC network sub-circuits. The model supports multiple field plate configurations and includes quantum mechanical effects like charge centroid shift, improving the accuracy of gate capacitance modeling. Tested against measured data, the ASM-HEMT model has shown excellent agreement with experimental results, confirming its reliability and precision in simulating GaN HEMT devices.

However, ASM-HEMT model has been found to not perform accurately at cryogenic temperatures [97][98][116], and this observation suggested making essential modifications to achieve experimentally accurate results under such conditions. Studies have shown that modifications are required to extend the model's accuracy to cryogenic temperatures to account for the trapping effect and charge-based flicker noise specific to low-temperature environments [115][116].

The steps involved in simulating the GaN HEMT device using ngspice are illustrated in Figure 3.7. This figure outlines the process, starting with the ASM-HEMT Verilog-A model, compiling it using the OpenVAF compiler to produce an OSDI file, and then using the ngspice simulator to run the simulation. Finally, the simulation results and the graphs are generated.

In conclusion, the integration of the ASM-HEMT model with ngspice and the use of Verilog-A for model development enable accurate and efficient simulation of GaN HEMT devices.

3.5.1 DC Analysis of HEMT at Room Temperature

DC analysis of the HEMT is required to see the device performance in different gate voltage regions. Also, it is important parameter to decide gate bias voltage and drain-source voltage level of the preamplifier circuit. To conduct the DC analysis of the HEMT at room temperature, the following steps were implemented using ngspice.

First, the ASM-HEMT Verilog-A model was compiled using the OpenVAF compiler. The compiled ASM-HEMT model was then included in the SPICE script. Subsequently, the circuit depicted in Figure 3.8 was constructed within the SPICE script.

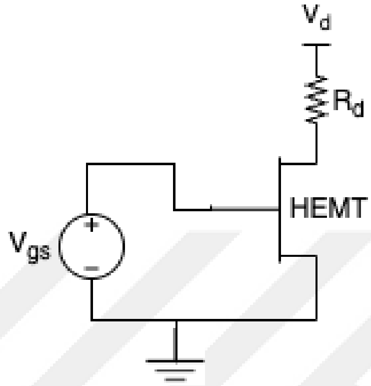

Figure 3.8: Circuit Diagram for DC analysis of HEMT

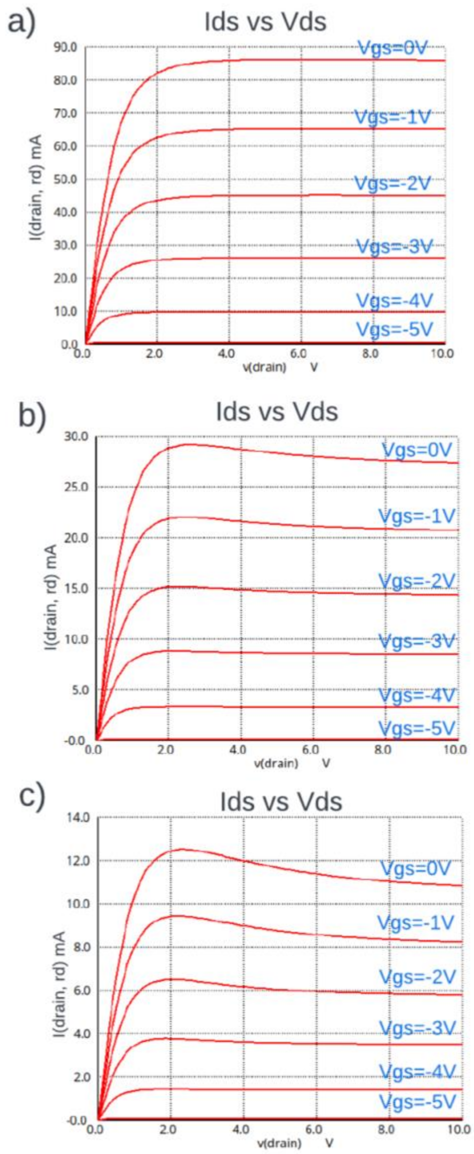

Figure 3.9: DC characteristics of the DUT at room temperature with a device length of 50 µm: output characteristics for gate widths of (a) 1 µm, (b) 3 µm, and (c) 7 µm with V_{GS} varying from 0V to -5V.

Simulations were performed for gate widths of 1 µm, 3 µm, and 7 µm, keeping the device length fixed at 50 µm. For each gate width, the I_{DS} vs. V_{DS} graph was plotted for 6 different V_{GS} values from 0V to -5V. The results showed that increasing the gate width led to a decrease in I_{DS} current. These findings are illustrated in Figure 3.9.

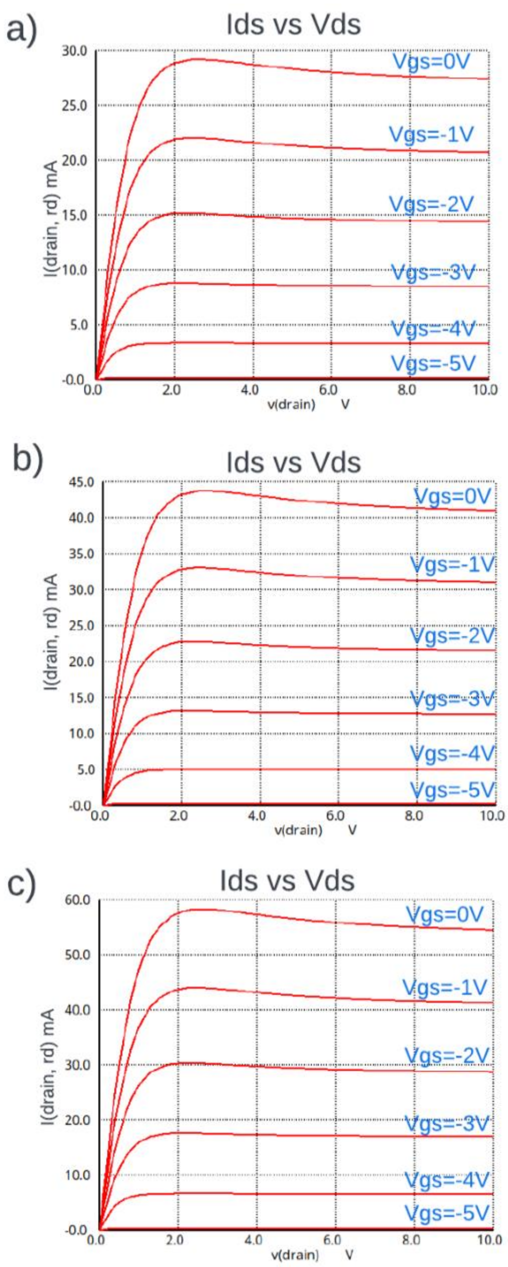

Figure 3.10: DC characteristics of the DUT at room temperature with a gate width of 3 µm: output characteristics for device lengths of (a) 50 µm, (b) 75 µm, and (c) 100 µm with V_{GS} varying from 0V to -5V.

Next, the gate width was fixed at 3 µm, and the same simulation was repeated for device lengths of 50 µm, 75 µm, and 100 µm. It was observed that increasing the device length resulted in an increase in I_{DS} current. These findings are illustrated in Figure 3.10.

In conclusion, the DC analysis of the ASM-HEMT at room temperature, combined with the exploration of different device geometries, confirmed that the model functions correctly within ngspice. The simulations validated the effects of gate width and device length on I_{DS} current, demonstrating the model's accuracy and reliability.

3.5.2 Applying Required Modifications to ASM-HEMT for Cryogenic Temperatures

The standard ASM-HEMT model does not accurately reflect the behavior of HEMTs at cryogenic temperatures, as shown in various studies [97][98]. In the study conducted by Nazir et al. [115], modifications to the ASM-HEMT model were proposed to improve the accuracy of low field mobility and threshold voltage calculations, aligning them more closely with experimental data at cryogenic temperatures.

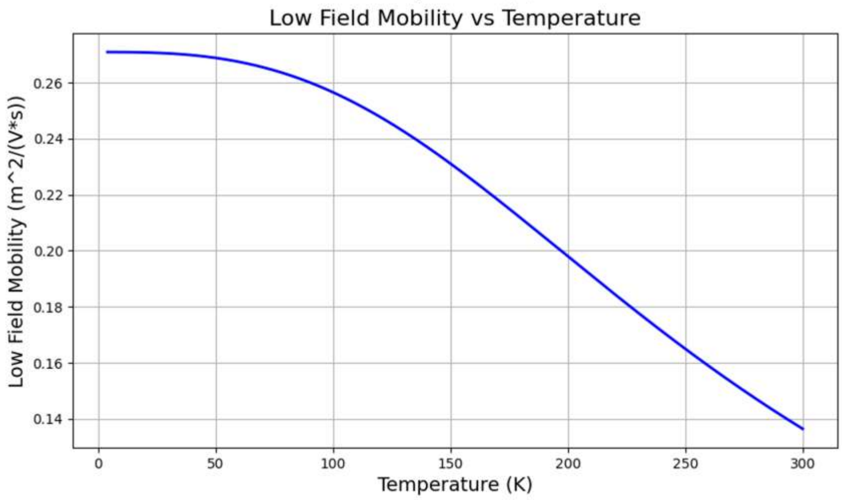

Figure 3.11: Characterizing Low Field Mobility Across Temperature Ranges

To adjust the low field mobility, the following formulation was employed:

$$\mu_{LF}(T) = \frac{\mu(T)}{[1 + \left(\frac{\mu(T)}{\mu_{Max}}\right)^{d_u}]^{(\frac{1}{d_u})}} \lambda u_T \qquad (3.1)$$

Here, μ_{Max} represents the maximum mobility, set at 0.271 m²/V·s. The temperature-dependent mobility $\mu(T)$ is given by $\mu_0(T_{DEV}/T_{NOM})^{\alpha_u}$. Parameters μ_0 (mobility at $T_{DEV} = T_{NOM}$), α_u, and $\lambda u_T = (1 + \alpha\Delta T)$ are varied to capture the temperature dependence. The parameter d_u governs the saturation temperature for mobility. After this change in low mobility calculation, the Low Field Mobility Across Temperature Ranges graph is given in

Figure 3.11.

For threshold voltage, the existing model expresses temperature dependence as:

$$V_{TH} = V_{TH0} - KT1(T_{DEV}/T_{NOM} - 1) \quad (3.2)$$

However, experimental results indicate that threshold voltage saturates at lower temperatures, whereas the existing model shows a linear increase with decreasing temperature. To address this discrepancy, an effective device temperature T_{EFF} is used instead of T_{DEV} in the threshold voltage expression:

$$V_{TH} = V_{TH0} - KT1(T_{EFF}/T_{NOM} - 1) \quad (3.3)$$

Here, V_{TH0} is the threshold voltage at $T_{EFF} = T_{NOM}$ and $KT1$ is a fitting parameter. The effective temperature T_{EFF} is defined as:

$$T_{EFF} = 0.5\left(T_{DEV} + T_S + \sqrt{(T_{DEV} - T_S)^2 + \Delta^2}\right) \quad (3.4)$$

This effective temperature formulation helps capture the saturation behavior of the subthreshold swing (SS) by replacing the thermal voltage $V_T = KT_{DEV}/q$ with $V_T = KT_{EFF}/q$ where K is Boltzmann's constant (in eV/K) and q is the electron charge. The temperature T_S marks the onset of SS saturation, and Δ is a smoothing parameter for the transition. All extracted parameter values are provided in Table 3.2.

Table 3.2: The extracted parameters for the device. [94]

Parameter	Value
μ_0 (m^2/V.S)	165.2e-3
α_u	-1.6
A	40e-3
μ_{max} (m^2/V.S)	270.9e-3
d_μ	1.8
V_{TH0} (V)	-5.05
KT1	354.0e-3
$\boldsymbol{T_S}$ (K)	100
Δ (K)	401.4

By implementing these modifications, the ASM-HEMT model can accurately simulate the behavior of GaN HEMT devices at cryogenic temperatures, ensuring that the simulation results closely match experimental observations. After implementing these changes, the modified ASM-HEMT Verilog-A code is compiled using OpenVAF to generate a new OSDI file.

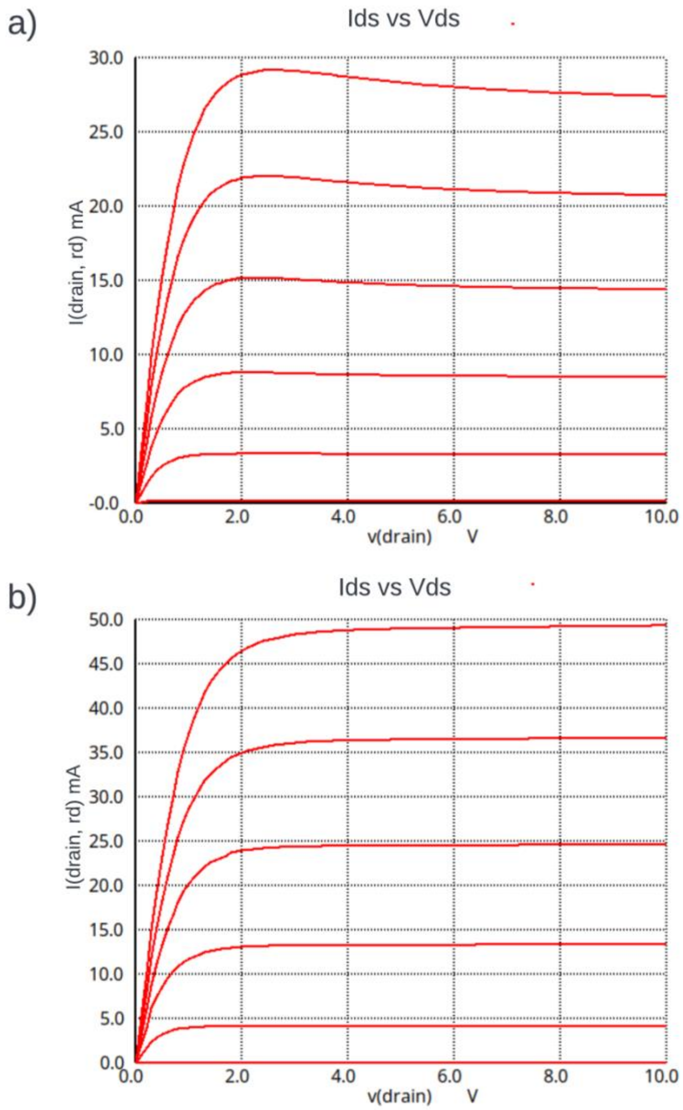

Figure 3.12: DC characteristics of the DUT at 4.2 Kelvin with a gate width of 3 µm and a device length of 50 µm. (a) shows the output characteristics using the unmodified ASM-HEMT model, while (b) displays the improved results with the modified ASM-HEMT model, indicating a 75% increase in $I_{DS,max}$ value from 28 mA to 49 mA.

In the SPICE script[117], the operating temperature is set to 4.2 K, and the simulation is run using the modified ASM-HEMT model. The simulations demonstrated a significant improvement, with the $I_{DS,max}$ value increasing from 28 mA to 49 mA, corresponding to a 75% increase. This enhancement is confirmed by the experimental results, which also show a 75% increase in the $I_{DS,max}$ value. Figure 3.12(a) illustrates the incorrect results obtained using the unmodified model, while Figure 3.12(b) shows the corrected results using the modified ASM-HEMT model.

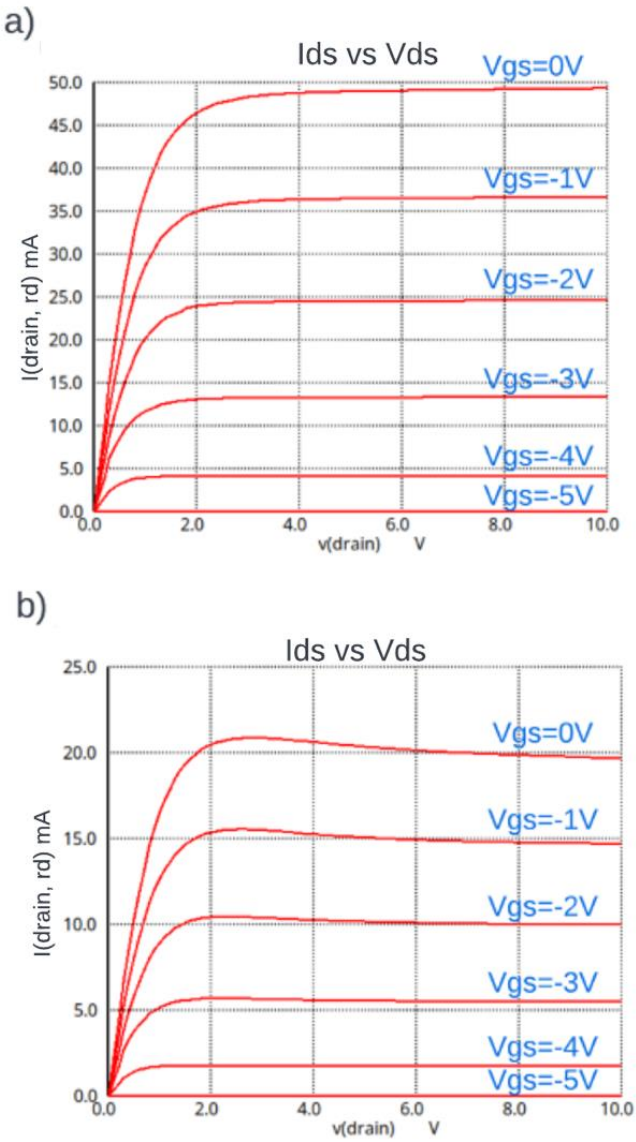

Figure 3.13: DC characteristics of the DUT at 4.2 Kelvin with a device length of 50 µm: output characteristics for gate widths of (a) 3 µm, and (b) 7 µm with V_{GS} varying from 0V to -5V.

Furthermore, we explored the effect of different gate widths on the HEMT's performance. Simulations were conducted for gate widths of 3 µm and 7 µm. The results, presented in Figure 3.13, show the performance at 4.2 K for gate widths of 3 µm (a), and 7 µm (b). Notably, the simulations revealed that reducing the gate width led to higher I_{DS} currents, demonstrating enhanced device performance with smaller gate dimensions.

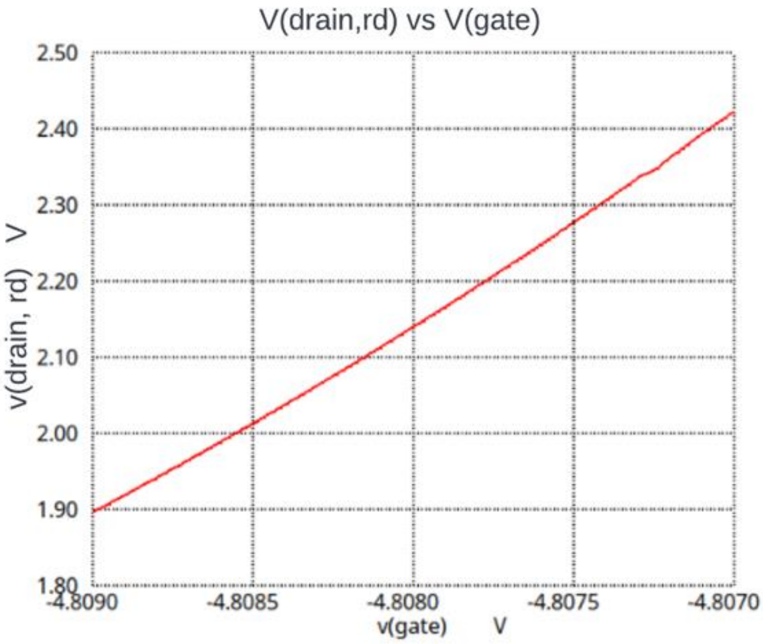

Figure 3.14: Voltage Response of $V_{drain,rd}$ Across R_D to Changes in V_{gate}

The effect of changes in gate voltage on the voltage drop across the drain resistor has also been investigated. For this purpose, the voltage across R_D was measured while increasing the gate voltage from -4.809 volts to -4.807 volts. Under these conditions, the voltage drop across R_D as a function of V_{gate} is presented in Figure 3.14. According to the simulation, a 2mV change in V_{gate} resulted in a 526mV change in the voltage drop across R_D. This indicates that the designed HEMT has a gain of 263 times, which corresponds to 48.39 dB. This significant gain demonstrates the preamplifier's high sensitivity and efficiency in amplifying signals under the specified operating conditions.

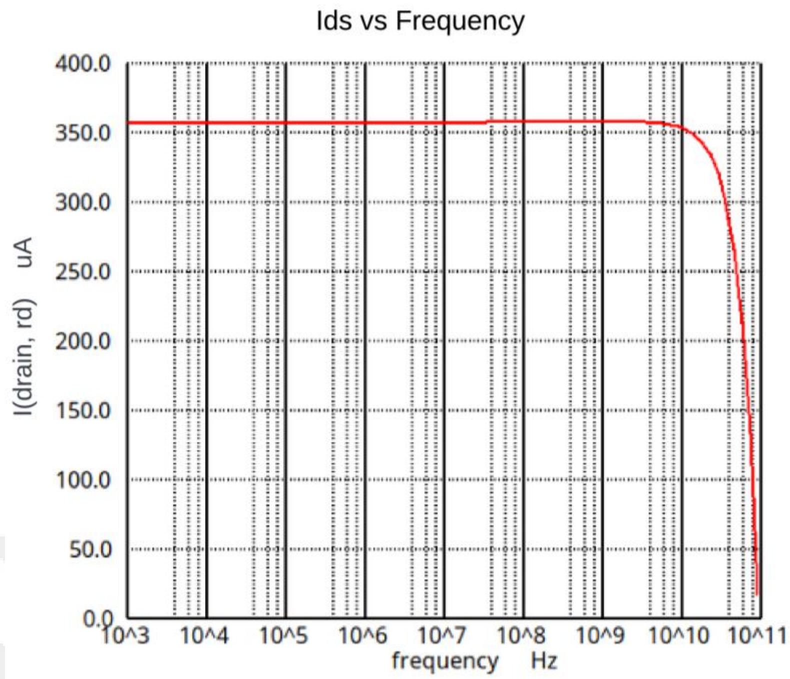

Figure 3.15: Frequency-Dependent Behavior of Drain Voltage in Modified ASM-HEMT on a Logarithmic Scale at 4.2 Kelvin

Finally, a frequency sweep simulation was conducted to observe the amplification gain of the designed cryogenic amplifier in different frequency. The result graph of the frequency sweep simulation is depicted in Figure 3.15. A sinusoidal signal was applied to the gate, extending up to 100 GHz, and the resulting current through I_{DS} was plotted to assess device performance across varying frequencies. It was observed that the HEMT maintained stable I_{DS} performance up to 10 GHz without any notable degradation. Additionally, the device exhibited a 3 dB decline in performance at 48.3 GHz, thereby establishing the cutoff frequency at 48.3 GHz.

3.6 *Layout Design of GaN HEMT Device*

The layout design of the GaN HEMT device was accomplished using KLayout, a powerful tool for layout creation and manipulation. The process began by defining the necessary layers using Python scripting within KLayout. Each layer corresponds to a different aspect of the device geometry. The script was meticulously crafted to draw the design of each layer according to the specified device geometry.

After defining the layers and creating the layout, the design was saved in the GDS format, which is widely used for semiconductor manufacturing. This format ensures that the design can be easily transferred to fabrication tools. The final 2D view of the designed GaN HEMT device is illustrated in Figure 3.16, providing a comprehensive visual representation of the device layout.

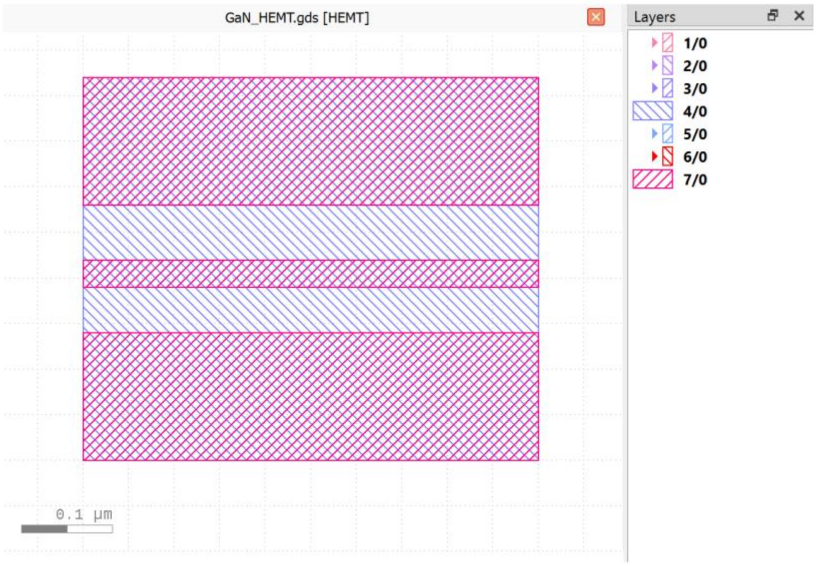

Figure 3.16: 2D Top View of Designed GaN HEMT Device

To enhance the visualization of the designed GaN HEMT device, the 2D layout was converted into a 2.5D view. This transformation involved creating a script that specified the thickness of each layer, effectively adding a third dimension to the design. The resulting 2.5D view is depicted in Figure 3.17, offering a detailed perspective of the designed device with the added depth dimension.

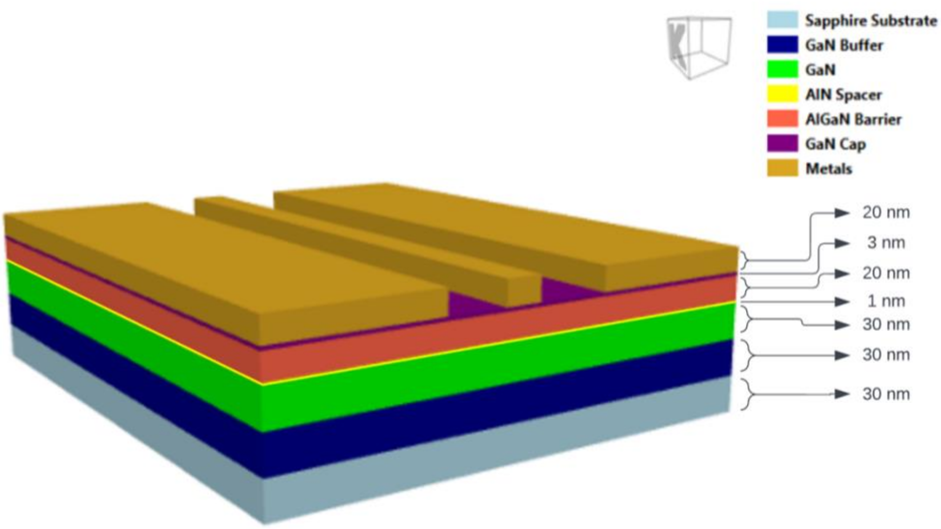

Figure 3.17: 2.5D View of Designed HEMT Device

3.7 *Conclusion*

In this chapter, the focus was on investigating the use of GaN HEMTs in cryogenic preamplifier circuits for SNSPD sensors. The ASM-HEMT SPICE model was employed to analyze the geometry determined from the literature review in SPICE simulations. However, it was found that the ASM-HEMT model did not provide values close to experimental results at cryogenic temperatures, as observed in studies from the literature. To address this issue, necessary model modifications were applied to accurately represent the behavior at cryogenic temperatures, and the model was compiled with OpenVAF to produce output in OSDI format.

Then, the modified ASM-HEMT model was included in ngspice, and DC analysis was performed, followed by observing the IDS current as a function of frequency. The simulations demonstrated that the modified model achieved up to 75% higher $I_{DS,max}$ values at cryogenic temperatures compared to room temperature, consistent with experimental results. Additionally, it was observed that the HEMT maintained stable I_{DS} performance up to 10 GHz without any notable degradation. The device exhibited a 3 dB decline in performance at 48.3 GHz, establishing the cutoff frequency at this point.

Chapter 4:
DESIGN AND INTEGRATION OF SNSPD READOUT CIRCUIT

Cryogenic preamplifiers are critical components in the field of low-temperature electronics, playing an essential role in a variety of applications such as quantum computing, superconducting detectors, and deep space communication. These preamplifiers are designed to operate efficiently at extremely low temperatures, often around 4.2 K, to amplify weak signals without introducing significant noise or distortion. One notable application of cryogenic preamplifiers is in superconducting nanowire single-photon detectors (SNSPDs).

Traditionally, amplification is done at room temperature, with signals transmitted from the cryogenic environment of the SNSPDs to the amplifiers via long coaxial cables. However, this setup has significant drawbacks. The long cables introduce signal degradation, increased noise, and timing jitter, which can severely impact the performance of the system. To overcome these challenges, integrating the amplifier directly into the cryogenic environment is preferred. This integration results in a more compact and efficient SNSPD readout system, reducing insertion loss and signal interference while maintaining low power consumption and high signal integrity.

Conventional preamplifiers, especially those utilizing silicon bipolar junction transistors (BJTs) and CMOS technologies, encounter substantial performance issues at cryogenic temperatures. Silicon BJTs, for example, experience a significant reduction in current gain (β), rendering them ineffective for use in cryogenic conditions [118].

CMOS circuits, although generally more stable, face significant challenges related to power dissipation. Some studies have observed that the cooling capacities of cryogenic infrastructures and the efficiency of heat transfer from circuits to coolants impose strict limitations on power distribution [119]. On the other hand, some studies have shown that cryogenic cooling significantly reduces the resistance of GaN HEMTs [88]. As a result, GaN HEMTs can operate with lower power consumption at cryogenic temperatures.

For SNSPD readout circuits, the ability to operate at high frequencies is crucial, as SNSPDs can achieve high count rates of up to 1.5 GHz. GaN HEMTs have been observed to exhibit faster switching speeds compared to SiC MOSFETs at cryogenic temperatures, making them more suitable for high-frequency applications [120]. Additionally, the higher transconductance of GaN HEMTs at low temperatures results in higher dv/dt and/or di/dt, allowing for increased switching frequencies [120].

High-fidelity readout is another crucial component of any superconducting-based system, imposing strict requirements on the noise performance of the readout chain [121][122]. Studies have demonstrated that at cryogenic temperatures, the output phase shift of GaN HEMTs decreases, which is vital for high-performance applications. Conversely, CMOS devices at cryogenic temperatures can experience signal distortion due to the "kink effect" caused by residual current [119]. These findings underscore the superior performance of GaN HEMTs in maintaining high signal fidelity at low temperatures compared to other technologies [122].

Another critical advantage of GaN HEMTs in cryogenic environments is their reduced system complexity. The lower on-resistance allows for higher current operation with fewer devices, simplifying the overall circuit design and reducing the number of components needed [120]. This reduction in complexity not only enhances reliability but also contributes to lower power consumption, a vital factor in cryogenic systems because of the limited cooling power of dilution refrigerators [25].

In summary, the use of GaN HEMT-based preamplifiers in cryogenic environments addresses the limitations of conventional preamplifier technologies by offering superior noise performance, higher frequency capabilities, and reduced system complexity. These advantages make them indispensable in advancing the capabilities of cryogenic electronics, particularly in fields demanding high precision and low noise.

In this chapter, a preamplifier circuit has been designed to operate at cryogenic temperatures for SNSPD sensors. The circuit employs the GaN HEMT device designed in Chapter 3. Using an effective circuit model, we design and analyze the preamplifier circuit through DC and AC SPICE simulations in Chapter 4. Finally, we investigate the maximum estimated power consumptions for single and parallel GaN HEMT preamplifiers in order to investigate the power dissipation of the preamplifier is still in the limits of the cooling power of the dilution refrigerator.

4.1 Overview of SNSPD Sensor Modeling

In the realm of SPICE simulations for Superconducting Nanowire Single Photon Detectors (SNSPDs), an equivalent circuit model is utilized to effectively simulate the behavior of the device upon photon detection.

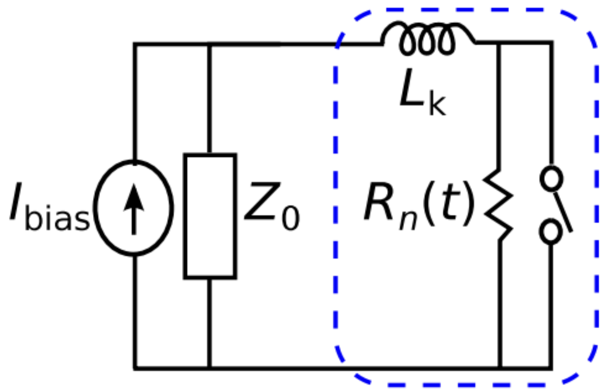

Figure 4.1: A simple electrical equivalent circuit of a SNSPD. L_k is the kinetic inductance of the superconducting nanowire and R_n is the hotspot resistance of the SNSPD. The SNSPD is current biased at I_{bias}. Opening and closing the switch simulates the absorption of a photon. An output pulse is measured across the load resistor Z_0. [99]

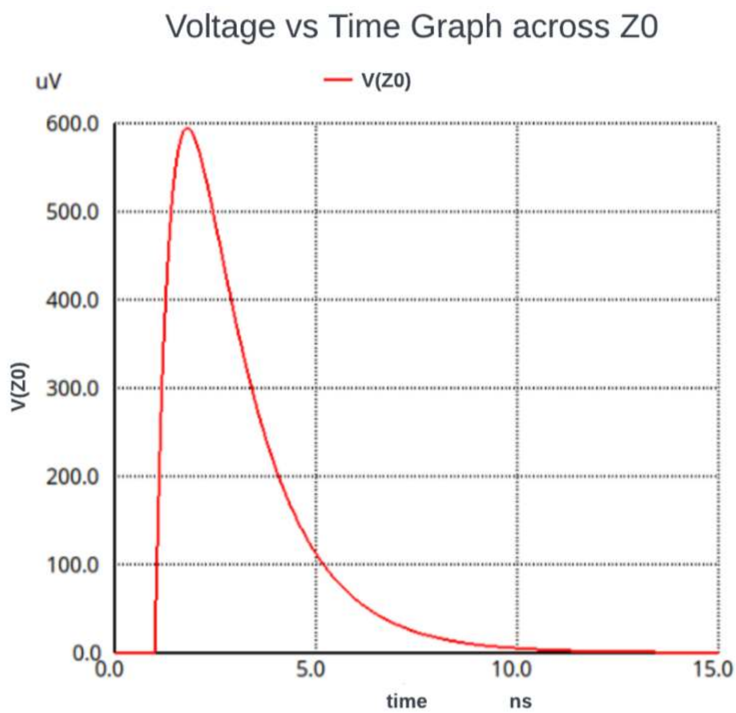

Figure 4.2: Time-Domain Simulation of Photon Detection in the SNSPD Equivalent Circuit Using SPICE. $V(Z_0)$represents the voltage difference across Z_0.

For modeling the voltage output of an SNSPD in response to an incident photon within SPICE simulations, the equivalent circuit shown in Figure 4.1 has been established. In this circuit, R_n represents the hotspot resistance of the SNSPD, and L_k denotes the kinetic inductance of the superconducting nanowire. The equivalent circuit includes a voltage-controlled switch to simulate the transition of the nanowire to a resistive state upon photon detection. A voltage pulse exceeding the threshold value is applied to the control input of the switch, representing the incident photon. This setup generates the SNSPD signal, as depicted in Figure 4.2, where the voltage across Z_0 is measured, capturing the characteristic response of the detector.

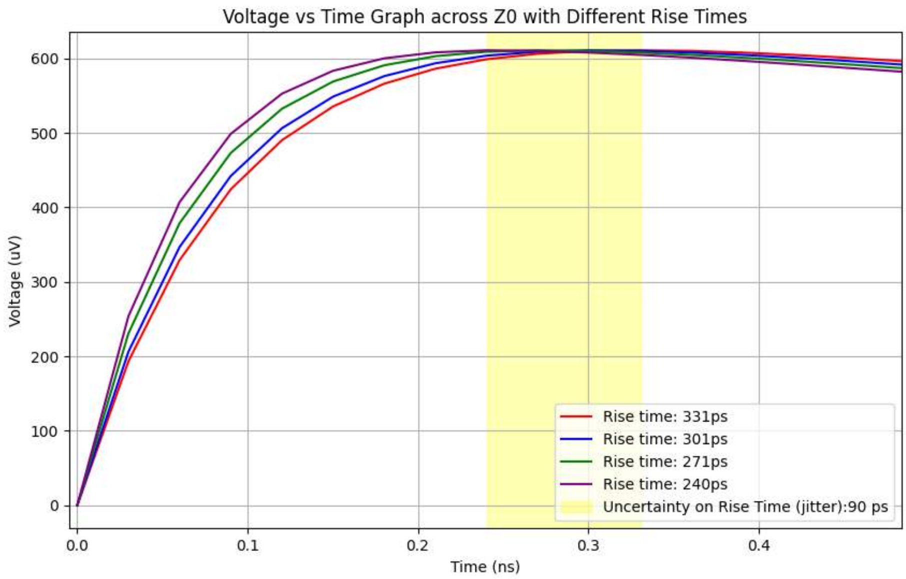

Figure 4.3: Time-Domain Simulation of Photon Detection in the SNSPD Equivalent Circuit with Different Rise Time

The uncertainty in the rise time of the SNSPD's voltage output is referred to as timing jitter. This timing jitter can be influenced by various factors, including the design of the detector, the properties of the materials used, and the operational parameters under which the detector is functioning [125]. Figure 4.3 illustrates the output signal of the equivalent SNSPD sensor model with four different rise time values. The variations in rise time are marked as uncertainty within the yellow shaded region.

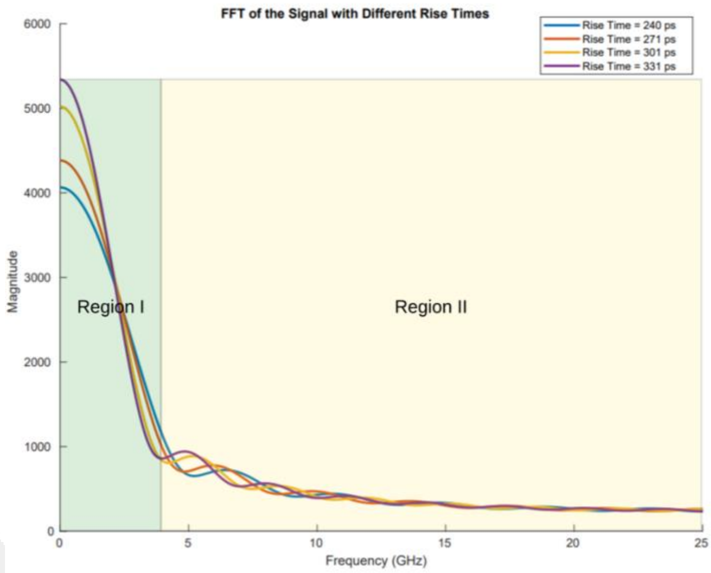

Figure 4.4: Frequency domain analysis of SNSPD signals with different rise times. Region I shows the meaningful part of the signal, while Region II captures the high-frequency noise caused by the steep rise of the signals.

Figure 4.4 presents the frequency domain representation of four SNSPD signals with varying rise times. This variability in rise times for the same sensor is what defines timing jitter. The uncertainty in rise time causes variations in the output signal of the SNSPD, leading to shifts in the detected time of incoming photons. A steep rise time corresponds to a high frequency in the frequency domain. To prevent this from appearing as noise in the output signal, it is crucial that these high-frequency components remain outside the operational bandwidth range [123]. The relatively high-frequency components observed in Region II can be disregarded in the operational bandwidth, allowing for a cleaner signal at the amplifier output. Therefore, it is crucial to appropriately configure the amplifier's operational frequency band to match the characteristics of the SNSPD sensor.

4.2 *Preamplifier Design Integration*

Given the critical role of the preamplifier in handling the typically 600-µV output signals produced by Superconducting Nanowire Single Photon Detectors (SNSPDs), it is essential to ensure that this component provides a gain exceeding 20 dB, thereby assuring that the output signal swing is sufficiently large for efficient processing by the post-analog-to-digital conversion circuitry[100][101][102].

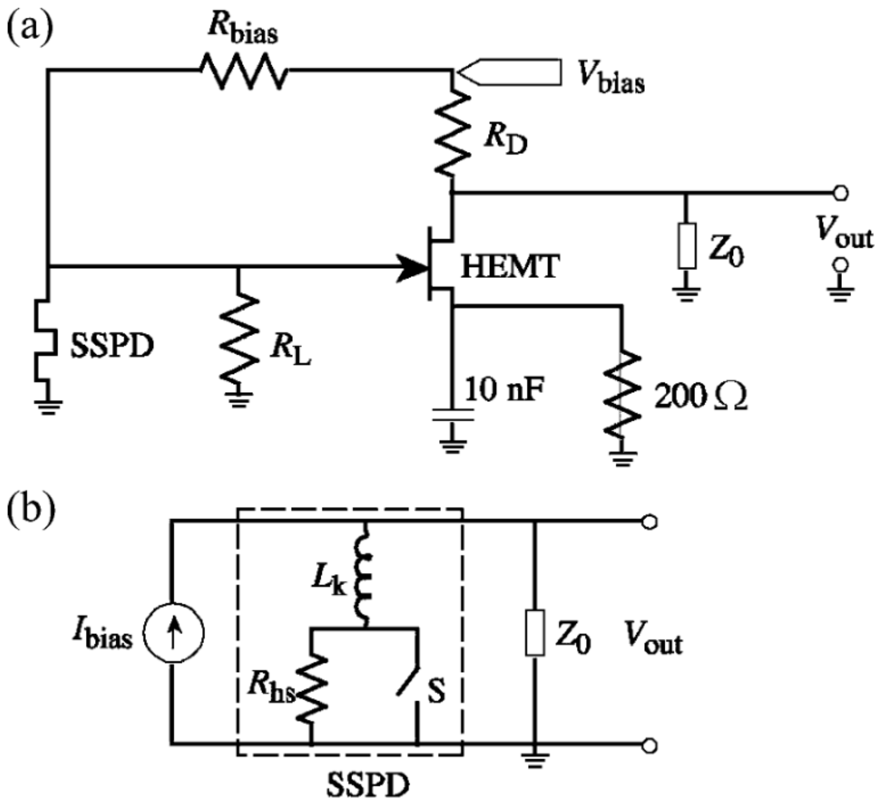

Figure 4.5: (a) Circuit schematics implementing HEMT amplifier and 500 Ohm load resistor. The 10-nF capacitor sets the maximum ac gain and a 200 Ohm resistor sets the dc current for the HEMT; and are the biasing and pull-up resistors, respectively. (b) Standard electrical photoresponse model of the SSPD with S denoting the detector switching action. Z_0=50 Ohm [103]

GaN HEMTs, known for their high input impedance and substantial gain, were selected for a single-stage preamplifier design in this study. An extensive literature review led to the adoption of a preamplifier circuit previously utilized by J. Kitaygorsky et al. [103], which is depicted in Figure 4.5. The high input impedance characteristic of the HEMT design enabled the determination of input impedance using an R_{Load} resistor. By adjusting the R_{bias} value, the HEMT's gate input can be set to the desired operating bias voltage. Additionally, the amplified signal output can be measured through Z_0. The IDS-VDS graph obtained from the HEMT DC simulation conducted at cryogenic temperatures was used to set the gate bias voltage at -4.63 volts. To achieve this voltage, the R_{bias} resistance value was precisely set to 32k ohms, ensuring the necessary conditions for optimal device performance under cryogenic conditions. An important practical consideration is grounding of the preamplifier circuit at the ground of the 3K stage, not higher temperature ground planes. This measure is essential to avoid unintentional current flow between ground planes at different temperature stages due to thermoelectric or thermocouple effects. An important practical consideration is grounding of the preamplifier circuit at the ground of the 3K stage, not higher temperature ground planes. This measure is essential to avoid unintentional current flow between ground planes at different temperature stages due to thermoelectric or thermocouple effects.

The power consumption of the designed GaN HEMT preamplifier circuit was also analyzed using simulation results, and it was measured that the system has a power dissipation of 1.2 mW while actively operating. If 300 mW, which is 20% of the 1.5W cooling power provided by the dilution refrigerator, is allocated for the preamplifier circuit, this result indicates that more than 200 preamplifiers can be accommodated within the dilution refrigerator. This allows for the use of the preamplifier with multipixel SNSPDs, which started getting developed recently [126].

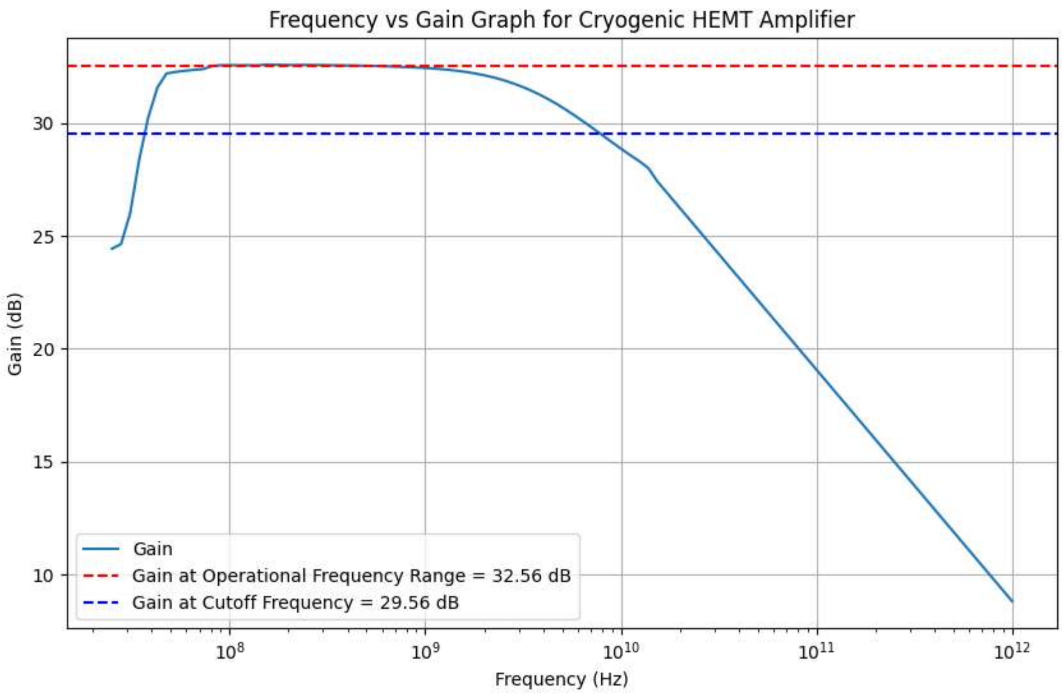

Figure 4.6: Frequency Response of Cryogenic GaN HEMT Amplifier

To observe the performance of the designed preamplifier circuit at different frequencies, a frequency-dependent gain analysis was conducted. An SNSPD signal was applied to the input of the preamplifier, and the output voltage was measured to calculate the gain. The resulting graph from this simulation is presented in Figure 4.6. It was observed that the preamplifier achieved a gain of 32.56 dB around 1 GHz. However, at 8 GHz, the gain decreased by 3 dB, dropping to 29.56 dB, indicating a cutoff frequency of 8 GHz.

Table 4.1: Comparison of Cryogenic Preamplifier Gain and Power Consumption Across Various Studies

References	[134]	[133]	[28]	This Work
Technology	SiGe	GaAs	SiGe	GaN
Gain (dB)	29.6	15	26	32.56
Power Consumption (mW)	20	2.5	1.6	1.2

Table 4.1 provides a comparison of the gain and power consumption values of the cryogenic preamplifier designed in this study with those of cryogenic preamplifiers from other works. As seen in the table, the cryogenic GaN HEMT preamplifier circuit simulated in this study delivers a higher gain while also exhibiting lower power consumption. These results indicate that GaN HEMTs show great promise for use in cryogenic preamplifier circuits. However, it is important to validate these findings through real-world testing.

Typical time-dependent SNSPD characteristics range from ps to ns rise time, 6-50 ps jitter [60][123] and their operation frequencies are around 1 GHz [59][124]. The operation bandwidth of the GaN HEMT devices designed here are greater than twice the range of operation frequencies. Besides, for building high-frequency analog-to-digital converters based on GaN HEMT devices, the bandwidth is high enough to support sampling the statistics of rise and fall time jitter of SNSPDs. The GaN HEMT electronics design here is not a bottleneck for the high-speed SNSPD operations for quantum telecommunication networks. These findings substantiate the suitability of the HEMT design for implementation in fast SNSPD’s, aligning with their operational requirements.

Chapter 5:
CONCLUSION AND FUTURE WORK

In this chapter, we present a summary of our findings and provide recommendations for future research. The "Summary of Findings" section consolidates the key insights gained from our study on High Electron Mobility Transistors (HEMTs), including their physical principles, design considerations, and performance metrics. The "Recommendations for Future Research" section outlines potential areas for further investigation to advance the understanding and application of HEMTs, particularly in cryogenic readout electronics.

5.1 Summary of Findings

In this study, a preamplifier circuit was designed for operation at cryogenic temperatures (4.2K), specifically for use with SNSPD (Superconducting Nanowire Single-Photon Detectors) sensors, and its performance was analyzed using SPICE simulations.

SNSPD sensors require cryogenic temperatures to function, typically achieved using dilution refrigerators. These sensors detect incoming photons and produce an electrical signal. However, this electrical signal suffers RF insertion and transmission losses when delivered out of the dilution refrigerator. To address this issue, earlier studies suggest placing a preamplifier circuit close to the SNSPD. This circuit requires semiconductor devices that operate effectively at cryogenic temperatures [27].

Upon reviewing various semiconductor options, GaN HEMT devices have been found to potentially outperform other semiconductor device types at low temperatures due to their high performance, high input impedance, and low output impedance. GaN HEMTs exhibit higher thermal conductivity, leading to lower power dissipation. Their high electron mobility prevents issues like kink effect and carrier freeze-out, commonly observed in other semiconductors at low temperatures. Consequently, the performance of a preamplifier circuit designed with GaN HEMTs was investigated in this study. The ASM-HEMT SPICE model was utilized for simulation, but it required modifications for accurate low-temperature operation. Modifications proposed by Nazir et al. [115] were applied to the ASM-HEMT model and compiled using OpenVAF, creating an OSDI format for use in ngspice.

DC analysis of the modified ASM-HEMT model was performed at cryogenic temperatures, measuring the IDS current. The simulation results confirmed an increase in IDS current by 75%, consistent with literature findings. Further DC analysis with varying gate widths and lengths determined that a gate width of 2 µm and device length of 50 µm provided optimal performance.

Subsequent AC analysis assessed the amplification performance across frequencies. The GaN HEMT maintained switching performance up to 10 GHz exhibited a cutoff frequency at 48.3 GHz, validating its suitability for the 1 GHz operating frequency required by SNSPD sensors. This wide bandwidth might benefit other applications such as quantum photonic integrated circuits, high-frequency quantum communication networks, space telecommunication networks, and other high-speed sensing and metrology applications.

An electrical model for the SNSPD was developed for SPICE simulation, and its output was tested. A preamplifier circuit incorporating the designed GaN HEMT was then built, and its signal amplification performance was analyzed. The SPICE simulation yielded a gain of 48.3 dB, exceeding the desired 20 dB gain noted in the literature for SNSPD applications.

Based on earlier promising studies [103], a preamplifier circuit was selected for the designed HEMT. The simplicity of the preamplifier circuit ensures it contains fewer components while capturing the effective inductive, capacitive and real impedance characteristics of the amplifier. This results in fewer components inside the dilution refrigerator and lower power dissipation, which helps maintain the dilution refrigerator's cooling power limit and ensures it operates at the necessary temperatures.

The chosen preamplifier circuit was assembled, and the resistance values were tuned, followed by gain measurements. It was observed that the preamplifier achieved a gain of 32.56 dB around 1 GHz. However, at 8 GHz, the gain decreased by 3 dB, dropping to 29.56 dB, indicating a cutoff frequency of 8 GHz.

Subsequently, a power consumption analysis was performed, and it was calculated that the designed preamplifier circuit has a power dissipation of 1.2 mW. If 300 mW, which is 20% of the 1.5W cooling power provided by the dilution refrigerator, is allocated for the preamplifier circuit, this result indicates that more than 200 preamplifiers can be accommodated within the dilution refrigerator. This observation suggests that recently emerging multichannel SNSPDs [124] and SNSPD-based cameras [126] can be integrated with the preamplifier for each pixel or detector column array or row.

This study concludes that GaN HEMT devices are highly effective in preamplifier circuits designed for SNSPD sensors operating at cryogenic temperatures, meeting all necessary performance criteria. The findings underscore that GaN HEMTs are excellent candidates for use in cryogenic SNSPD readout circuits, promising enhanced reliability and efficiency in these specialized applications.

5.2 *Recommendations for Future Research*

This study has successfully implemented SPICE simulations to explore the performance of GaN HEMT devices in preamplifier circuits for SNSPD sensors. However, to further validate these findings, it is recommended to proceed with a tape-out followed by a thorough examination of experimental results. For this purpose, epitaxial growth and testing of GaN HEMT devices and experimental confirmation of the models presented here are going to be essential in the future. One way to achieve high-quality GaN HEMT device fabrication is through getting GaN foundry services. These services might allow for fabricating the layers with pre-optimized recipes that would allow for near-ideal device operation characteristics. Below is a list of GaN foundries, which might be able to fabricate the proposed GaN HEMT devices.

Table 5.1: Some of the GaN foundries that provide growth and fabrication services for GaN-based epilayers and devices

Company	Country	Ref.
MACOM	USA	[127]
QROMIS	USA	[128]
Trusted Semiconductor Solutions	USA	[129]
X-FAB	Germany (Germany, France, Malaysia, USA)	[130]
Sanan IC	China	[131]

These results are essential for the fine calibration of GaN HEMT characteristics, ensuring that the simulated outcomes closely align with real-world performance.

Additionally, detailed noise analysis is advised to enhance the understanding of noise characteristics in these circuits. This would provide crucial insights into the noise contributions from GaN HEMTs and their impact on the overall sensor performance, particularly under low-signal conditions.

Further characterization of GaN HEMTs on different substrates such as SiC, silicon or other strained substrates should also be considered. Exploring various substrate materials could reveal significant variations in device performance and durability, which are critical for optimizing the design and functionality of SNSPD systems.

There is also a need for targeted development of preamplifier circuits specifically designed for particular types of SNSPD sensors. Such tailored designs could significantly improve sensor responses under varied operating conditions, including dark conditions. Alongside, conducting dark count analysis and assessing detection efficiency will provide a comprehensive understanding of the sensor behavior in absence of light, which is vital for low-light applications.

Efforts were made to use the open-source TCAD program DEVSIM for simulating the GaN HEMT device. Although the physics of the HEMT could be modeled, an overflow error occurred in DEVSIM's matrix solutions at low temperatures. This issue was due to the significant changes in parameters as the temperature decreased, leading to very large values in the calculations. Future research could address this problem by modifying the simulator to handle these conditions or by using alternative simulators capable of accurately performing TCAD simulations for HEMT devices at cryogenic temperatures.

Improving GaN HEMT bandwidth: For broader sensing or communication applications that require broader bandwidths, GaN HEMT geometry must also be optimized for lower RC constants and effective capacitances. Increasing the device length and reducing the gate width increases the I_{DS}, which helps increase the signal at higher frequencies and increase the operation bandwidth. Tuning the HEMT capacitances might also help in optimizing their cut-off frequencies.

Clear characterization of the effect of gate bias voltage: When gate bias voltage is applied, the 2DEG carrier concentration is changed in a nonlinear manner. Hence, the device current-voltage characteristics must be solved self-consistently in numerical models. These models need to be tested and verified with experiments.

Commercial and room temperature applications: GaN HEMT device applications are not just limited in quantum sensing, computing or communications. GaN HEMT devices have a wide range of commercially viable room temperature applications in consumer, industrial, and automotive sectors due to their highest efficiency and power density. These HEMT devices can withstand up to 700V bias and can form the basis of DC converters, adapters, and battery charger modules. Major semiconductor companies such as Infineon are already offering significant GaN HEMT product lines for these purposes [132].

Reviewing the literature and considering the findings from this study, GaN HEMT devices emerge as promising candidates for cryogenic preamplifier circuits in SNSPD sensors. However, due to their relatively recent development compared to traditional Si-based MOSFETs, there is less existing research on HEMT devices. Further studies and advancements are crucial for improving single photon detection processes. Enhancing the understanding and application of GaN HEMTs in this field will be essential for achieving better performance and reliability in advanced photonics technology.

BIBLIOGRAPHY

[1] P. Colinge et al., “Temperature effects on trigate SOI MOSFETs,” IEEE Electron Device Letters, vol. 27, no. 3, pp. 172–174, Mar. 2006, doi: 10.1109/LED.2006.869941.

[2] Chen, H. Elgabra, C.-H. Chen, J. Baugh, and L. Wei, “Estimation of MOSFET Channel Noise and Noise Performance of CMOS LNAs at Cryogenic Temperatures,” in 2021 IEEE International Symposium on Circuits and Systems (ISCAS), May 2021, pp. 1–5. doi: 10.1109/ISCAS51556.2021.9401136.

[3] E. Charbon et al., “Cryo-CMOS for quantum computing,” in 2016 IEEE International Electron Devices Meeting (IEDM), Dec. 2016, p. 13.5.1-13.5.4. doi: 10.1109/IEDM.2016.7838410.

[4] A. Grill *et al.*, “Reliability and Variability of Advanced CMOS Devices at Cryogenic Temperatures,” in *2020 IEEE International Reliability Physics Symposium (IRPS)*, Dallas, TX, USA: IEEE, Apr. 2020, pp. 1–6. doi: 10.1109/IRPS45951.2020.9128316.

[5] V. Desmaris, D. Meledin, E. Sundin, M. Thorsell, N. Rorsman, and V. Belitsky, “Characterization of GaN-based Low Noise Amplifiers at Cryogenic Temperatures,” 2019.

[6] H. Zhang *et al.*, “Compositionally graded III-nitride alloys: building blocks for efficient ultraviolet optoelectronics and power electronics,” *Rep. Prog. Phys.*, vol. 84, no. 4, p. 044401, Apr. 2021, doi: 10.1088/1361-6633/abde93.

[7] H. Guo, J. Zhou, M. Wang, and X. Zou, “Output Phase and Amplitude Analysis of GaN-Based HEMT at Cryogenic Temperatures,” *IEEE Microw. Wireless Compon. Lett.*, vol. 31, no. 11, pp. 1219–1222, Nov. 2021, doi: 10.1109/LMWC.2021.3079222.

[8] Gisin, G. G. Ribordy, W. Titel, H. Zbinden, “Quantum Cryptography” Reviews of Modern Physics, 74, 145-195 (2002)

[9] A. Hiskett, D. Rosenberg, C. G. Peterson, R. J. Hughes, S. Nam, A. E. Lita, A. J. Miller, and J. E. Nordholt. “Long-distance quantum key distribution in optical fibre,” New J. Phys. 8, 193 (2006)

[10] Knill, R. Laflamme, and G. J. Milburn, “A scheme for efficient quantum computation with linear optics,” Nature 409, 46-52 (2001).

[11] L. Migdal, D. Branning, and S. Castelletto, "Tailoring single-photon and multiphoton probabilities of a singlephoton on-demand source", Phys. Rev. A 66, 053805 (2002).

[12] A. Lampert, L. A. Chewter, David. Phillips, D. V. O'Connor, A. J. Roberts, and S. R. Meech, "Standards for nanosecond fluorescence decay time measurements," Anal. Chem., vol. 55, no. 1, pp. 68–73, Jan. 1983, doi: 10.1021/ac00252a020.

[13] Henri Dautet, Pierre Deschamps, Bruno Dion, Andrew D. MacGregor, Darleene MacSween, Robert J. McIntyre, Claude Trottier, and Paul P. Webb, "Photon counting techniques with silicon avalanche photodiodes," Appl. Opt. 32, 3894-3900 (1993)

[14] Cabrera, R. M. Clarke, P. Colling, A. J. Miller, S. Nam, and R. W. Romani, "Detection of single infrared, optical, and ultraviolet photons using superconducting transition edge sensors," Appl. Phys. Lett., vol. 73, no. 6, pp. 735–737, 1998.

[15] E. Lita, B. Calkins, L. A. Pellouchoud, A. J. Miller, and S. Nam, "Superconducting transition-edge sensors optimized for high-efficiency photon-number resolving detectors," presented at the SPIE Defense, Security, and Sensing, M. A. Itzler and J. C. Campbell, Eds., Orlando, Florida, Apr. 2010, p. 76810D. doi: [10.1117/12.852221](https://doi.org/10.1117/12.852221).

[16] Stasi, G. Gras, R. Berrazouane, M. Perrenoud, H. Zbinden, and F. Bussières, "High-efficiency and fast photon-number resolving parallel superconducting nanowire single-photon detector," Phys. Rev. Applied, vol. 19, no. 6, p. 064041, Jun. 2023, doi: 10.1103/PhysRevApplied.19.064041.

[17] H. K. Onnes, Commun. Phys. Lab Univ. Leiden. Suppl., vol. 29, 1911.

[18] Md. Atikur Rahman, "A Review on Cuprate Based Superconducting Materials Including Characteristics and Applications," *AJPA*, vol. 3, no. 2, p. 39, 2015, doi: 10.11648/j.ajpa.20150302.15.

[19] A. Abdallah Ahmed Elfaki, "The Effect of Temperature on Conductivity of Conductors and Superconductors," Am. J. Phys. Appl., vol. 5, no. 1, p. 1, 2017.

[20] J. R. Kirtley, "Fundamental studies of superconductors using scanning magnetic imaging," Reports Prog. Phys., vol. 73, no. 12, 2010.

[21] Bardeen, J.; Cooper, L. N., Schrieffer, J. R. (April 1957). "Microscopic Theory of Superconductivity". Physical Review 106 (1): 162–164. Bardeen, J.; Cooper, L. N.; Schrieffer, J. R. (December 1957). "Theory of Superconductivity". Physical Review 108 (5): 1175– 1204.

[22] Cooper, Leon N. (1956). "Bound electron pairs in a degenerate Fermi gas". Physical Review 104 (4): 1189– 1190.

[23] F. B. Silsbee, “A note on electrical conduction in metals at low temperatures,” Journal of the Washington Academy of Sciences, vol. 6, no. 17, pp. 597–602, 1916.

[24] Sharma, R.G. (2021). The Phenomenon of Superconductivity and Type II Superconductors. In: Superconductivity. Springer Series in Materials Science, vol 214. Springer, Cham. https://doi.org/10.1007/978-3-030-75672-7_2

[25] Krinner *et al.*, “Engineering cryogenic setups for 100-qubit scale superconducting circuit systems,” *EPJ Quantum Technol.*, vol. 6, no. 1, p. 2, Dec. 2019, doi: 10.1140/epjqt/s40507-019-0072-0.

[26] Bluefors cryogenics. http://www.bluefors.com/. Accessed: Jul. 04, 2024.

[27] P. Kurpiers, T. Walter, P. Magnard, Y. Salathe, and A. Wallraff, “Characterizing the attenuation of coaxial and rectangular microwave-frequency waveguides at cryogenic temperatures,” EPJ Quantum Technol., vol. 4, no. 1, p. 8, Dec. 2017, doi: 10.1140/epjqt/s40507-017-0059-7.

[28] X. Niu, L. Li, X. Wu, and D. Wang, “A Wideband Cryogenic Readout Amplifier with Temperature-Insensitive Gain for SNSPD,” *Sensors*, vol. 22, no. 3, p. 1225, Feb. 2022, doi: 10.3390/s22031225.

[29] A. Grill et al., “Reliability and Variability of Advanced CMOS Devices at Cryogenic Temperatures,” in 2020 IEEE International Reliability Physics Symposium (IRPS), Dallas, TX, USA: IEEE, Apr. 2020, pp. 1–6. doi: 10.1109/IRPS45951.2020.9128316.

[30] J.-P. Colinge et al., “Temperature effects on trigate SOI MOSFETs,” IEEE Electron Device Lett., vol. 27, no. 3, pp. 172–174, Mar. 2006, doi: 10.1109/LED.2006.869941.

[31] Finn, J. Yuan, R. Krithivasan, L. Najafizadeh, P. Cheng, and J. D. Cressler, “A 10 Mbps SiGe BiCMOS Transceiver for Operation Down to Cryogenic Temperatures,” in 2007 IEEE Bipolar/BiCMOS Circuits and Technology Meeting, Sep. 2007, pp. 115–118. doi: 10.1109/BIPOL.2007.4351849.

[32] Yao, F. Dai, R. C. Jaeger, and J. D. Cressler, “A 12-Bit Cryogenic and Radiation-Tolerant Digital-to-Analog Converter for Aerospace Extreme Environment Applications,” IEEE Transactions on Industrial Electronics, vol. 55, no. 7, pp. 2810–2819, Jul. 2008, doi: 10.1109/TIE.2008.924174.

[33] C. Bardin et al., "A high-speed cryogenic SiGe channel combiner IC for large photon-starved SNSPD arrays," in 2013 IEEE Bipolar/BiCMOS Circuits and Technology Meeting (BCTM), Sep. 2013, pp. 215–218. doi: 10.1109/BCTM.2013.6798179.

[34] Ulaganathan et al., "A sige BiCMOS instrumentation channel for extreme environment applications," VLSI Des., vol. 2010, p. 3:1-3:12, Jan. 2010, doi: 10.1155/2010/156829.

[35] Liang Q, Cressler JD, Niu G, Malladi RM, Newton K, Harame DL. A physics-based high-injection transit-time model applied to barrier effects in SiGe HBTs. IEEE Trans Electron Dev 2002;49:1807.

[36] Joseph AJ, Cressler JD, Richey DM, Harame DL. Impact of profile scaling on high-injection barrier effects in advanced UHV/CVD SiGe HBTs. In: IEEE int electron device meeting 1996, Symp-1996. p. 253.

[37] B. Nguyenphu, "SiGe Technology for Military and Deep Space Cryogenic Power Electronics," in AIP Conference Proceedings, Keystone, Colorado (USA): AIP, 2006, pp. 359–366. doi: 10.1063/1.2192372.

[38] H. Ying et al., "Operation of SiGe HBTs Down to 70 mK," IEEE Electron Device Lett., vol. 38, no. 1, pp. 12–15, Jan. 2017, doi: 10.1109/LED.2016.2633465.

[39] A. T.-J. Lee, "A low-power-dissipation broadband cryogenic preamplifier utilizing GaAs MESFETs in parallel," Review of Scientific Instruments, vol. 64, no. 8, pp. 2373–2378, Aug. 1993, doi: 10.1063/1.1143938.

[40] N. Islam, M. F. P. Mohamed, M. F. A. J. Khan, S. Falina, H. Kawarada, and M. Syamsul, "Reliability, Applications and Challenges of GaN HEMT Technology for Modern Power Devices: A Review," Crystals, vol. 12, no. 11, p. 1581, Nov. 2022, doi: 10.3390/cryst12111581.

[41] Y. An, K. Ren, L. Yin, and J. Zhang, "Modeling on Monolithic Integration Structure of AlGaN/InGaN/GaN High Electron Mobility Transistors and LEDs: 2DEG Density and Radiative Recombination," Electronics, vol. 12, no. 5, p. 1087, Feb. 2023, doi: 10.3390/electronics12051087.

[42] D. Pavlidis, "HBT vs. PHEMT vs. MESFET: What's best and why".

[43] Christopher Harris, Raymond Pengelly, S Sheppard, T Smith, B Pribble, S Wood, and C Platis. Commercial gan devices for switching and low noise applications. In CS MANTECH Conference, 2011.

[44] G. Orr, M. Azoulay, G. Golan, and A. Burger, “GaN HEMT based high energy particles detection preamplifier.” arXiv, Jun. 23, 2021. Accessed: Jul. 04, 2024. [Online]. Available: http://arxiv.org/abs/2106.12703

[45] H. Hadfield, “Single-photon detectors for optical quantum information applications,” Nature Photon, vol. 3, no. 12, pp. 696–705, Dec. 2009, doi: 10.1038/nphoton.2009.230.

[46] F. Zappa, S. Tisa, A. Tosi, S. Cova, "Principles and features of single-photon avalanche diode arrays," Sensors and Actuators A: Physical, vol. 140, no. 1, pp. 103-112, 2007.

[47] Vines, P., Kuzmenko, K., Kirdoda, J. et al. High performance planar germanium-on-silicon single-photon avalanche diode detectors. Nat Commun 10, 1086 (2019). https://doi.org/10.1038/s41467-019-08830-w

[48] C. Niclass, et al., "Design and characterization of a CMOS 3-D image sensor based on single photon avalanche diodes," IEEE Journal of Solid-State Circuits, vol. 40, no. 9, pp. 1847-1854, 2005.

[49] O. Thomas, Z. L. Yuan, J. F. Dynes, A. W. Sharpe, and A. J. Shields, “Efficient photon number detection with silicon avalanche photodiodes,” Applied Physics Letters, vol. 97, no. 3, p. 031102, Jul. 2010, doi: 10.1063/1.3464556.

[50] Makoto Akiba, Kenji Tsujino, and Masahide Sasaki, "Ultrahigh-sensitivity single-photon detection with linear-mode silicon avalanche photodiode," Opt. Lett. 35, 2621-2623 (2010)

[51] Irwin KD, Hilton GC. "Transition-edge sensors." In: Topics Appl. Phys. vol. 99. Berlin: Springer; 2005.

[52] Irwin KD. "An application of electrothermal feedback for high resolution cryogenic particle detection." Appl Phys Lett.

[53] X-ray Testbed for Breakthrough Catalyst Measurements. https://www.nist.gov/. Accessed: 2023-07-05.

[54] J. Bardeen, L. N. Cooper, and J. R. Schrieffer, "Theory of superconductivity," Phys. Rev., vol. 108, no. 5, pp. 1175–1204, 1957.

[55] B. Cabrera, R. M. Clarke, P. Colling, A. J. Miller, S. Nam, and R. W. Romani, "Detection of single infrared, optical, and ultraviolet photons using superconducting transition edge sensors," Appl. Phys. Lett., vol. 73, no. 6, pp. 735–737, 1998.

[56] A. E. Lita, B. Calkins, L. A. Pellouchoud, A. J. Miller, and S. Nam, "Superconducting transition-edge sensors optimized for high-efficiency photon-number resolving detectors," presented at the SPIE Defense, Security, and Sensing, M. A. Itzler and J. C. Campbell, Eds., Orlando, Florida, Apr. 2010, p. 76810D. doi: 10.1117/12.852221.

[57] K. K. Berggren, Q. Y. Zhao, N. Abebe, M. Chen, P. Ravindran, A. McCaughan, and J. C. Bardin, "A superconducting nanowire can be modeled by using SPICE," Superconductor Science and Technology, vol. 31, no. 5, 2018. doi: 10.1088/1361-6668/aab149

[58] G. N. Gol'tsman, O. Okunev, G. Chulkova, A. Lipatov, A. Semenov, K. Smirnov, B. Voronov, A. Dzardanov, C. Williams, and R. Sobolewski, "Picosecond superconducting single-photon optical detector," Applied Physics Letters, vol. 79, no. 6, pp. 705–707, 2001. doi: 10.1063/1.1388868

[59] Kristine M. Rosfjord, Joel K. W. Yang, Eric A. Dauler, Andrew J. Kerman, Vikas Anant, Boris M. Voronov, Gregory N. Gol'tsman, and Karl K. Berggren, "Nanowire Single-photon detector with an integrated optical cavity and anti-reflection coating," Opt. Express 14, 527-534 (2006)

[60] Divochiy, A., Marsili, F., Bitauld, D. et al. Superconducting nanowire photon-number-resolving detector at telecommunication wavelengths. Nature Photon 2, 302–306 (2008). https://doi.org/10.1038/nphoton.2008.51

[61] Adriana E. Lita, Aaron J. Miller, and Sae Woo Nam, "Counting near-infrared single-photons with 95% efficiency," Opt. Express 16, 3032-3040 (2008)

[62] R. Dixon, Z. L. Yuan, J. F. Dynes, A. W. Sharpe, and A. J. Shields, "Gigahertz decoy quantum key distribution with 1 Mbit/s secure key rate," Opt. Express 16, 18790-18797 (2008)

[63] D. Rosenberg, A. E. Lita, A. J. Miller, and S. W. Nam, "Noise-free high-efficiency photon-number-resolving detectors," Physical Review A 71, 061803 (2005).

[64] Rosenberg et al., "Long-Distance Decoy-State Quantum Key Distribution in Optical Fiber," Phys. Rev. Lett., vol. 98, no. 1, p. 010503, Jan. 2007, doi: 10.1103/PhysRevLett.98.010503.

[65] M. Natarajan, M. G. Tanner, and R. H. Hadfield, "Superconducting nanowire single-photon detectors: physics and applications," Supercond. Sci. Technol., vol. 25, no. 6, p. 063001, Jun. 2012, doi: 10.1088/0953-2048/25/6/063001.

[66] Marsili et al., “Detecting single infrared photons with 93% system efficiency,” Nature Photon, vol. 7, no. 3, Art. no. 3, Mar. 2013, doi: 10.1038/nphoton.2013.13.

[67] Chaolin Lv, Weijun Zhang, Lixing You, Peng Hu, Heqing Wang, Hao Li, Chengjun Zhang, Jia Huang, Yong Wang, Xiaoyan Yang, Zhen Wang, Xiaoming Xie; Improving maximum count rate of superconducting nanowire single-photon detector with small active area using series attenuator. AIP Advances 1 October 2018; 8 (10): 105018. https://doi.org/10.1063/1.5049549

[68] C. Cahall, D. J. Gauthier, and J. Kim, “Scalable cryogenic readout circuit for a superconducting nanowire single-photon detector system,” Review of Scientific Instruments, vol. 89, no. 6, p. 063117, Jun. 2018, doi: 10.1063/1.5018179.

[69] A. N. McCaughan, “Readout architectures for superconducting nanowire single photon detectors,” Supercond. Sci. Technol., vol. 31, no. 4, p. 040501, Apr. 2018, doi: 10.1088/1361-6668/aaa1b3.

[70] T. Mimura, N. Yokoyama, H. Kusakawa, K. Suyama, and M. Fukuta, “MP-A4 GaAs MOSFET for low-power high-speed logic applications,” IEEE Trans. Electron Devices, vol. ED-26, no. 11, pp. 1828–1828, Nov. 1979.

[71] T. Mimura, “The early history of the high electron mobility transistor (HEMT),” IEEE Trans. Microwave Theory Techn., vol. 50, no. 3, pp. 780–782, Mar. 2002, doi: 10.1109/22.989961.

[72] M. A. Khan, A. Bhattarai, J. N. Kuznia, and D. T. Olson, “High electron mobility transistor based on a GaN-Alx Ga1−x N heterojunction,” Appl. Phys. Lett., vol. 65, no. 9, pp. 1121–1123, 1993.

[73] A. M. Nahhas, “Review of AlGaN/GaN HEMTs Based Devices,” American Journal of Nanomaterials.

[74] T. J. Reck, W. Deal and G. Chattopadhyay, "Cryogenic performance of HEMT amplifiers at 340GHz and 670GHz," 2014 IEEE MTT-S International Microwave Symposium (IMS2014), Tampa, FL, USA, 2014, pp. 1-3, doi: 10.1109/MWSYM.2014.6848250.

[75] D. Delagebeaudeuf and N. T. Linh, "Metal-(n) AlGaAs-GaAs two-dimensional electron gas FET," in IEEE Transactions on Electron Devices, vol. 29, no. 6, pp. 955-960, June 1982, doi: 10.1109/T-ED.1982.20813.

[76] J. Shanthi and D. P. Vimala, “High Electron Mobility Transistor: A Review on Analytical Models,” vol. 3, no. 05.

[77] A. . -J. Shey and W. H. Ku, "An analytical current-voltage characteristics model for high electron mobility transistors based on nonlinear charge-control formulation," in IEEE Transactions on Electron Devices, vol. 36, no. 10, pp. 2299-2306, Oct. 1989, doi: 10.1109/16.40914.

[78] J. Zolper, "A review of junction field effect transistors for hightemperature and high power electronics," Solid State Electron 42, 2153-2156 (1998).

[79] M. Alim, M. Ali, A. Rezazadeh, C. Gaquiere, "Thermal response for intermodulation distortion components of GaN HEMT for low and high frequency applications," Microelectronic Engineering 209, 53-59 (2019).

[80] T. R. Lenka, G. N. Dash and A. K. Panda, "2DEG transport characteristics by self-consistent subband calculations of Schrödinger and poisson equations in InAlN/GaN HEMT," 2014 IEEE 9th Nanotechnology Materials and Devices Conference (NMDC), Aci Castello, Italy, 2014, pp. 124-127, doi: 10.1109/NMDC.2014.6997438.

[81] O. Ambacher et al., "Two-dimensional electron gases induced by spontaneous and piezoelectric polarization charges in N- and Ga-face AlGaN/GaN heterostructures," Journal of Applied Physics, vol. 85, no. 6, pp. 3222–3233, Mar. 1999, doi: 10.1063/1.369664.

[82] E. T. Yu, G. J. Sullivan, P. M. Asbeck, C. D. Wang, D. Qiao, and S. S. Lau, "Measurement of piezoelectrically induced charge in GaN/AlGaN heterostructure field-effect transistors," Applied Physics Letters, vol. 71, no. 19, pp. 2794–2796, Nov. 1997, doi: 10.1063/1.120138.

[83] S. Colangeli, A. Bentini, W. Ciccognani, E. Limiti and A. Nanni, "GaN-based robust low-noise amplifiers", IEEE Trans. Electron Devices, vol. 60, no. 10, pp. 3238-3248, Oct. 2013.

[84] PPG Microsemi. Gallium nitride (GaN) versus silicon carbide (SiC) in the high frequency (RF) and power switching applications. Digi-key, 2014.

[85] Fan Ren and John C Zolper. Wide energy bandgap electronic devices. World Scientific, 2003.

[86] Peter J Wellmann. Power electronic semiconductor materials for automotive and energy saving applications–SiC, GaN, Ga2O3, and diamond. Zeitschrift für anorganische und allgemeine Chemie, 643(21):1312–1322, 2017.

[87] Malmros, A., Chen, J.-T., Hjelmgren, H., Lu, J., Hultman, L., Kordina, O., Sveinbjörnsson, E. Ö., Zirath, H., & Rorsman, N. (2019). Enhanced Mobility in

InAlN/AlN/GaN HEMTs Using a GaN Interlayer. IEEE Transactions on Electron Devices, 66(7), 2910–2915. https://doi.org/10.1109/TED.2019.2914674

[88] Nela, L., Perera, N., Erine, C., & Matioli, E. (2021). Performance of GaN Power Devices for Cryogenic Applications Down to 4.2 K. IEEE Transactions on Power Electronics, 36(7), 7412–7416. https://doi.org/10.1109/TPEL.2020.3047466

[89] Dae-Young Jeon, Yumin Koh, Chu-Young Cho, Kyung-Ho Park; Impact of temperature-dependent series resistance on the operation of AlGaN/GaN high electron mobility transistors. AIP Advances 1 November 2021; 11 (11): 115203. https://doi.org/10.1063/5.0064823

[90] Z. Zhang et al., "Characterization of Wide Bandgap Semiconductor Devices for Cryogenically-Cooled Power Electronics in Aircraft Applications," 2018 AIAA/IEEE Electric Aircraft Technologies Symposium (EATS), Cincinnati, OH, USA, 2018, pp. 1-8.

[91] Guo, H., Zhou, J., Wang, M., & Zou, X. (2021). Output Phase and Amplitude Analysis of GaN-Based HEMT at Cryogenic Temperatures. IEEE Microwave and Wireless Components Letters, 31(11), 1219–1222. https://doi.org/10.1109/LMWC.2021.3079222

[92] Dogmuş, E., Kabouche, R., Lepilliet, S., Linge, A., Zegaoui, M., Ben-Ammar, H., Chauvat, M.-P., Ruterana, P., Gamarra, P., Lacam, C., Tordjman, M., & Medjdoub, F. (2016). InAlGaN/GaN HEMTs at Cryogenic Temperatures. Electronics, 5(2), 31. https://doi.org/10.3390/electronics5020031

[93] Mebarki, M. A., Ferrand-Drake Del Castillo, R., Meledin, D., Sundin, E., Thorsell, M., Rorsman, N., Belitsky, V., & Desmaris, V. (2023). Noise Characterization and Modeling of GaN-HEMTs at Cryogenic Temperatures. IEEE Transactions on Microwave Theory and Techniques, 71(5), 1923–1931. https://doi.org/10.1109/TMTT.2022.3226480

[94] B. Zeng et al., “DC and low-frequency noise characteristics of GaN-based HEMTs under cryogenic temperatures,” J. Phys. D: Appl. Phys., vol. 55, no. 43, p. 434003, Oct. 2022, doi: 10.1088/1361-6463/ac89fc.

[95] A. Dasgupta, S. Ghosh, Y. S. Chauhan and S. Khandelwal, "ASM-HEMT: Compact model for GaN HEMTs," 2015 IEEE International Conference on Electron Devices and Solid-State Circuits (EDSSC), Singapore, 2015, pp. 495-498, doi: 10.1109/EDSSC.2015.7285159.

[96] Advanced SPICE Model for HEMTs Technical Manual. https://iitk.ac.in/. Accessed: Jul. 20, 2024.

[97] Wu, R. Yao, Y. Liu, K. Geng, and Y. Zhu, "An Extended Temperature Model Based on the Trapping Effect for Drain-Source Current in GaN HEMTs," Physica Status Solidi (a), vol. 221, no. 6, p. 2300783, Mar. 2024, doi: 10.1002/pssa.202300783.

[98] S. Nazir, A. Pampori, R. Dangi, S. A. Ahsan, and Y. S. Chauhan, "Charge-Based Flicker Noise Modeling of GaN HEMTs Down to Cryogenic Temperatures," IEEE Electron Device Lett., vol. 44, no. 9, pp. 1416–1419, Sep. 2023, doi: 10.1109/LED.2023.3294552.

[99] C. M. Natarajan, M. G. Tanner, and R. H. Hadfield, "Superconducting nanowire single-photon detectors: physics and applications," Supercond. Sci. Technol., vol. 25, no. 6, p. 063001, Jun. 2012, doi: 10.1088/0953-2048/25/6/063001.

[100] He, L.; Li, L.; Niu, X.; Haiyang, X.; Xie, M.; Wu, X.; Zhang, L.; Kang, L.; Wang, Z. A Low-Power, Inductorless Wideband Cryogenic Amplifier For Supercondcting Nanowire Single Photon Detector. IEEE Trans. Appl. Supercond. 2019, 29, 1–6.

[101] Bardin, J.; Weinreb, S. A 0.1-5 GHz cryogenic SiGe MMIC LNA. IEEE Microw. Wirel. Compon. Lett. 2009, 19, 407–409.

[102] Chang, S.-W.; Bardin, J. A Wideband cryogenic SiGe LNA MMIC with an average noise temperature of 2.8 K from 0.3-3 GHz. In Proceedings of the 2017 IEEE MTT-S International Microwave Symposium (IMS2017), Honolulu, HI, USA, 4–9 June 2017; pp. 157–159.

[103] Kitaygorsky, S. Dorenbos, E. Reiger, R. Schouten, V. Zwiller, and R. Sobolewski, "HEMT-Based Readout Technique for Dark- and Photon-Count Studies in NbN Superconducting Single-Photon Detectors," IEEE Trans. Appl. Supercond., vol. 19, no. 3, pp. 346–349, Jun. 2009, doi: 10.1109/TASC.2009.2018191.

[104] Jardndal, A.H., Large Signal Modelling of GaN Device for High Power Amplifier Design. 2007,University of Kassel: Kassel.

[105] I. A. Kuznetsova, D. N. Romanov, and O. V. Savenko, "Calculation electrical conductivity a two-dimensional electron gas of AlGaN/GaN-based transistors with high electron mobility," Phys. Scr., vol. 99, no. 8, p. 085917, Aug. 2024, doi: 10.1088/1402-4896/ad5b90.

[106] K. Yang, S. Nazir, M. Behtash, and J. Cheng, “High-Throughput Design of Two-Dimensional Electron Gas Systems Based on Polar/Nonpolar Perovskite Oxide Heterostructures,” Sci Rep, vol. 6, no. 1, p. 34667, Oct. 2016, doi: 10.1038/srep34667.

[107] S. Nazir, M. Behtash, & K. Yang, "Towards enhancing two-dimensional electron gas quantum confinement effects in perovskite oxide heterostructures", Journal of Applied Physics, vol. 117, no. 11, 2015. https://doi.org/10.1063/1.4915950

[108] S. Ozaki, J. Yaita, A. Yamada, Y. Kumazaki, Y. Minoura, T. Ohkiet al., "First demonstration of x-band algan/gan high electron mobility transistors using free-standing aln substrate over 15 w mm−1 output power density", Applied Physics Express, vol. 14, no. 4, p. 041004, 2021. https://doi.org/10.35848/1882-0786/abec90

[109] J. Kim, K. Choi, S. Lee, H. Park, & Y. Kwon, "6-18 ghz reactive matched gan mmic power amplifiers with distributed l-c load matching", Journal of Electromagnetic Engineering and Science, vol. 16, no. 1, p. 44-51, 2016. https://doi.org/10.5515/jkiees.2016.16.1.44

[110] P. Das, T. Wu, & S. Tallur, "Design and analysis of high electron mobility transistor inspired: iii-v electro-optic modulator topologies", Semiconductor Science and Technology, vol. 35, no. 9, p. 095028, 2020. https://doi.org/10.1088/1361-6641/ab9ea9

[111] S. Sharbati, I. Gharibshahian, T. Ebel, A. Orouji, & W. Franke, "Analytical model for two-dimensional electron gas charge density in recessed-gate gan high-electron-mobility transistors", Journal of Electronic Materials, vol. 50, no. 7, p. 3923-3929, 2021. https://doi.org/10.1007/s11664-021-08842-7

[112] K. Oreszczuk, "Enhancement of electron magnetic susceptibility due to many-body interactions in monolayer mose2", 2d Materials, vol. 10, no. 4, p. 045019, 2023. https://doi.org/10.1088/2053-1583/acefe3

[113] A. Kalavagunta, A. Touboul, L. Shen, R. Schrimpf, R. Reed, D. Fleetwoodet al., "Electrostatic mechanisms responsible for device degradation in algan/aln/gan hemts",, 2007. https://doi.org/10.1109/radecs.2007.5205538

[114] Y. Kong, M. Zhang, J. Zhou, Y. Zhang, K. Zhang, D. Penget al., "A 16 gs/s 3-bit dac core in gan hemt technology", Physica Status Solidi (A), vol. 215, no. 7, 2018. https://doi.org/10.1002/pssa.201700790

[115] M. S. Nazir, R. Dangi, M. Zaid, A. Pampori, and Y. S. Chauhan, “Extension of ASM-HEMT Framework for Cryogenic Temperatures,” in 2024 8th IEEE Electron

Devices Technology & Manufacturing Conference (EDTM), Bangalore, India: IEEE, Mar. 2024, pp. 1–3. doi: 10.1109/EDTM58488.2024.10512078.

[116] M. Mebarki, R. Castillo, D. Meledin, E. Sundin, M. Thorsell, N. Rorsmanet al., "Noise characterization and modeling of gan-hemts at cryogenic temperatures", Ieee Transactions on Microwave Theory and Techniques, vol. 71, no. 5, p. 1923-1931, 2023. https://doi.org/10.1109/tmtt.2022.3226480

[117] “bugratufan/gan_cryogenic_preamplifier: Design and Simulation of Readout Circuit for SNSPDs in Cryogenic Environments.” Accessed: Jul. 26, 2024. [Online]. Available: https://github.com/bugratufan/gan_cryogenic_preamplifier

[118] H. Gui et al., “Review of Power Electronics Components at Cryogenic Temperatures,” IEEE Trans. Power Electron., vol. 35, no. 5, pp. 5144–5156, May 2020, doi: 10.1109/TPEL.2019.2944781.

[119] E. Charbon, M. Babaie, A. Vladimirescu, and F. Sebastiano, “Cryogenic CMOS Circuits and Systems: Challenges and Opportunities in Designing the Electronic Interface for Quantum Processors,” IEEE Microwave, vol. 22, no. 1, pp. 60–78, Jan. 2021, doi: 10.1109/MMM.2020.3023271.

[120] R. Chen and F. F. Wang, “SiC and GaN Devices With Cryogenic Cooling,” IEEE Open J. Power Electron., vol. 2, pp. 315–326, 2021, doi: 10.1109/OJPEL.2021.3075061.

[121] T. Watson et al., “A programmable two-qubit quantum processor in silicon,” Nature, vol. 555, no. 7698, pp. 633–637, 2018. doi: 10.1038/ n at u r e 2 576 6 .

[122] H. Guo, J. Zhou, M. Wang, and X. Zou, “Output Phase and Amplitude Analysis of GaN-Based HEMT at Cryogenic Temperatures,” IEEE Microw. Wireless Compon. Lett., vol. 31, no. 11, pp. 1219–1222, Nov. 2021, doi: 10.1109/LMWC.2021.3079222.

[123] F. Garzetti, N. Lusardi, E. Ronconi, A. Costa, S. Velez, C. Gallandet al., "Assessment of the bundle snspd plus fpga-based tdc for high-performance time measurements", IEEE Access, vol. 10, p. 127894-127910, 2022. https://doi.org/10.1109/access.2022.3227462

[124] W. Zhang et al., "A 16-Pixel Interleaved Superconducting Nanowire Single-Photon Detector Array With A Maximum Count Rate Exceeding 1.5 GHz," in IEEE Transactions on Applied Superconductivity, vol. 29, no. 5, pp. 1-4, Aug. 2019, Art no. 2200204, doi: 10.1109/TASC.2019.2895621.

[125] R. Cheng, X. Guo, X. Ma, L. Fan, K. Fong, & H. Tang, "Self-aligned multi-channel superconducting nanowire single-photon detectors", Optics Express, vol. 24, no. 24, p. 27070, 2016. https://doi.org/10.1364/oe.24.027070

[126] L. Stasi, T. Taher, G. V. Resta, H. Zbinden, R. Thew, and F. Bussières, "High photon-number efficiencies with a fast 28-pixel parallel SNSPD," Jun. 21, 2024, arXiv: arXiv:2406.15312. Accessed: Jul. 26, 2024. [Online]. Available: http://arxiv.org/abs/2406.15312

[127] "Foundry & Design Services." Accessed: Jul. 26, 2024. [Online]. Available: https://www.macom.com/foundry-services

[128] "Qromis - Revolutionary substrates for LED, Power and RF." Accessed: Jul. 26, 2024. [Online]. Available: http://www.qromis.com/#secondPage

[129] "Services | Trusted Semiconductor Solutions Inc." Accessed: Jul. 26, 2024. [Online]. Available: https://trustedsemi.com/services-2/

[130] "SiC & GaN foundry solutions that fit your needs: X-FAB." Accessed: Jul. 26, 2024. [Online]. Available: https://www.xfab.com/technology/sic-gan

[131] "GaN Foundry-Sanan IC." Accessed: Jul. 26, 2024. [Online]. Available: https://www.sanan-ic.com/en/gan-foundry

[132] I. T. AG, "GaN transistors (GaN HEMTs) - Infineon Technologies." Accessed: Jul. 26, 2024. [Online]. Available: https://www.infineon.com/cms/en/product/power/gan-hemt-gallium-nitride-transistor/

[133] C. T. Cahall, D. J. Gauthier, and J. Kim, "Cryogenic Amplifiers for a Superconducting Nanowire Single Photon Detector System," in Conference on Lasers and Electro-Optics, Optica Publishing Group, 2016, p. JTu5A.26. doi: 10.1364/CLEO_AT.2016.JTu5A.26.

[134] S. Weinreb, J. C. Bardin and H. Mani, "Design of Cryogenic SiGe Low-Noise Amplifiers," in IEEE Transactions on Microwave Theory and Techniques, vol. 55, no. 11, pp. 2306-2312, Nov. 2007, doi: 10.1109/TMTT.2007.907729.

Appendix A: KLayout Scripts for 2D GDS File Generation and 2.5D Visualization

The Python script below was used to draw the GDS file according to the required physical length parameters. This script sets up the layout, defines the layers, and creates the shapes representing the various components of the HEMT device.

```
import pya
layout = pya.Layout()
layout.dbu = 0.001  # database unit in micrometers

layers = {
  "sapphire": layout.layer(1, 0, "Sapphire"),
  "gan_buffer": layout.layer(2, 0, "GaN Buffer"),
  "gan": layout.layer(3, 0, "GaN"),
  "aln": layout.layer(4, 0, "AlN"),
  "algan": layout.layer(5, 0, "AlGaN"),
  "cap": layout.layer(6, 0, "GaN Cap"),
  "metal": layout.layer(7, 0, "Metal"),
}

# Device dimensions in micrometers (width, length)
device_dimensions = {
  "width": 50,  # WG
  "length": 14  # LSD
}

gate_length = 3  # LG
source_length = 5  # Length for Source
drain_length = 5  # Length for Drain
gate_position = (device_dimensions["length"] - gate_length) / 2  # Center the gate

# Layer dimensions and positions
dimensions = {
  "sapphire": (0, 0, device_dimensions["width"], device_dimensions["length"]),
  "gan_buffer": (0, 0, device_dimensions["width"], device_dimensions["length"]),
  "gan": (0, 0, device_dimensions["width"], device_dimensions["length"]),
  "aln": (0, 0, device_dimensions["width"], device_dimensions["length"]),
  "algan": (0, 0, device_dimensions["width"], device_dimensions["length"]),
```

```
  "cap": (0, 0, device_dimensions["width"], device_dimensions["length"]),
  "metal": [
    (0, gate_position, device_dimensions["width"], gate_position + gate_length),  # Gate
    (0, 0, device_dimensions["width"], source_length),  # Source
    (0, device_dimensions["length"] - drain_length, device_dimensions["width"], device_dimensions["length"])
# Drain
  ]
}

# Create layers and insert shapes
cell = layout.create_cell("HEMT")
for name, layer in layers.items():
  layer_index = layer
  if name == "metal":
    for box in dimensions[name]:
      cell.shapes(layer_index).insert(pya.Box(*box))
  else:
    box = dimensions[name]
    cell.shapes(layer_index).insert(pya.Box(*box))

# Save the layout as GDS file
layout.write("GaN_HEMT.gds")
```

To view the layout generated by the 2D drawing script in a 2.5-dimensional perspective, the following script was used. This script allows for the visualization of the layout, enhancing the understanding of the device structure in three dimensions.

```
# 2.5D script for GaN HEMT structure visualization
z(input(1, 0), zstart: 0, height: 30.nm, fill: 0xADD8E6, name: "Sapphire Substrate")   # Sapphire substrate,
30 nm
z(input(2, 0), zstart: 30.nm, height: 30.nm, fill: 0x00008B, name: "GaN Buffer")
z(input(3, 0), zstart: 60.nm, height: 30.nm, fill: 0x00FF00, name: "GaN")
z(input(4, 0), zstart: 90.nm, height: 1.nm, fill: 0xFFFF00, name: "AlN Spacer")
z(input(5, 0), zstart: 91.nm, height: 20.nm, fill: 0xFF6347, name: "AlGaN Barrier")
z(input(6, 0), zstart: 111.nm, height: 3.nm, fill: 0x800080, name: "GaN Cap")
z(input(7, 0), zstart: 114.nm, height: 20.nm, fill: 0xDAA520, name: "Metals")
```